7-2016

Fabrication, characterization and skin permeation of antoxidant-loaded lipid vesicles for transdermal drug delivery.

Emily Martin
University of Louisville

Follow this and additional works at: https://ir.library.louisville.edu/etd

Part of the Biomedical Engineering and Bioengineering Commons

FABRICATION, CHARACTERIZATION, AND SKIN PERMEATION OF
ANTOXIDANT-LOADED LIPID VESICLES FOR TRANSDERMAL DRUG
DELIVERY

By

Emily Martin
B.S., University of Louisville, 2015

A Thesis
Submitted to the Faculty of the
University of Louisville
J.B. Speed School of Engineering
as Partial Fulfillment of the Requirements
for the Professional Degree

MASTER OF ENGINEERING

Department of Bioengineering

July 2016

FABRICATION, CHARACTERIZATION, AND SKIN PERMEATION OF
ANTOXIDANT-LOADED LIPID VESICLES FOR TRANSDERMAL DRUG
DELIVERY

Submitted by:_____
Emily Martin

A Thesis Approved On

_____
(Date)

By the Following Reading and Examination Committee:

_____
Dr. Patricia Soucy, Thesis Director

_____
Dr. William Ehringer

_____
Dr. Erin Gerber

iv

ACKNOWLEDGEMENTS

ABSTRACT

Excess production of Reactive Oxygen Species (ROS), which can be caused by radiation, cigarette smoke, and pollutants, can cause many damaging cellular effects, such as DNA damage and unregulated cell apoptosis. If left unmitigated, chronic overproduction of ROS has been linked to the formation of cancer, diabetes, atherosclerosis, rheumatoid arthritis, chronic inflammation, Parkinson's disease, Alzheimer's disease, multiple sclerosis, and amyotrophic lateral sclerosis. ROS is typically eliminated with antioxidants, which scavenge and inhibit the formation of ROS by becoming oxidized by the ROS and by binding to its precursors.

Curcumin is an effective lipid-soluble antioxidant agent. However, its poor bioavailability, rapid metabolism by the liver and intestinal tract, and short biological half-life greatly hinders its therapeutic abilities. The water soluble antioxidant, n-2-mercaptoproprionyl glycine (N-MPG), also has been found to scavenge ROS and decrease lipid peroxidation. Like curcumin, its therapeutic efficacy is limited due to its poor half-life. In order to improve bioavailability and stability of these two antioxidants, lipid vesicle formulations have been designed and characterized for transdermal delivery of the antioxidants. Transdermal delivery is a pain-free method of drug delivery that allows the antioxidants to permeate through the skin layers for systemic delivery.

Three lipid vesicle formulations, traditional liposomes, ultradeformable liposomes, and ethosomes, have been fabricated and characterized in order to determine which vesicle type has the highest skin permeation through the stratum corneum. Each of the three lipid vesicle formulations were composed of 10 mg/ml Soy-PC, 0.48 mg/ml

curcumin, and 1 mg/ml N-MPG. The ultradeformable vesicles incorporate an edge activator, 1.5 mg/ml cholic acid, into its structure to increase deformability of the vesicles. The ethosomes are vesicles composed in a 40% ethanol solution to increase the fluidity of the vesicles and skin membrane. The vesicles were characterized for size, stability, morphology, and entrapment efficiency. A modified Franz-Diffusion Chamber was used to test the skin permeability of each vesicle type.

Each particle type was fabricated to have a diameter less than 200 nm. The unloaded particle types were tested for stability using a PeroxiDetect Assay, which detected amount of lipid hydroperoxides. The ethosomes had the least amount while the ultradeformable liposomes had the most. However, when analyzing size of the vesicles over various time points, the ultradeformable liposomes were the most stable. Every vesicle type had a semi-spherical morphology, with the ultradeformable liposomes having the smoothest morphology. The ethosomes had the highest entrapment efficiency of curcumin (statistically similar to the traditional liposomes) and N-MPG.

The modified Franz-Diffusion chamber was used to characterize skin deposition of the vesicles. At hour 2, the ethosomes had the highest fluorescence and consequently, skin deposition. At hour 24, the traditional liposomes, which were statistically similar to the ultradeformable liposomes, had the highest skin deposition. In the image analysis, the ethosomes had the highest sum intensity in the stratum corneum. In the epidermis, the traditional liposomes, which were statistically similar to the ethosomes, had the highest sum intensity. The traditional liposomes had the highest sum intensity in the dermis layer. Subsequently, the ethosomes are recommended for short-term applications of curcumin and N-MPG while the traditional liposomes are recommended for long-term applications.

TABLE OF CONTENTS

NOMENCLATURE

DI = deionized
DLS = dynamic light scattering
EHT = extra high tension
EtOH = ethanol
FA = formaldehyde
FSU = fluorescent standard unit
GFP = green fluorescent protein
H&E = hematoxylin and eosin y
HBSS = Hank's balanced salt solution
N-MPG = n-2-mercaptoproprionyl glycine
PBS = phosphate buffered saline
ROS = reactive oxygen species
SEM = scanning electron microscope
Soy-PC = soya phosphatidylcholine

LIST OF TABLES

LIST OF FIGURES

I. INTRODUCTION

A. Background

Various cellular processes produce reactive oxygen species (ROS), an oxygen containing molecule with an unpaired electron in its outer orbit [1]. The most commonly produced cellular ROS molecules are hydroxyl (OH•) and superoxide (O_2^- •) [1]. These species can be endogenously formed through cellular respiration, respiratory burst, and enzymatic reactions. Exogenous production of ROS can occur via exposure to radiation, pollutants, cigarette smoke, food, and drugs [2]. Ionizing radiation creates ROS by radiolysis of water or other oxygen containing molecules [2]. Pollutants and cigarette smoke contain many highly reactive chemicals, leading to the generation of free radicals and ROS. Various food molecules, such as Fe^{2+}, trans fatty acids, phenols, and alcohols, can either destabilize chemical reactions to produce ROS or create free radicals upon chemical breakdown [2]. The introduction of drugs into the system, for treatments like glucocorticoid therapy or volatile anesthetics for surgery, can stimulate oxidative stress, forming ROS [2].
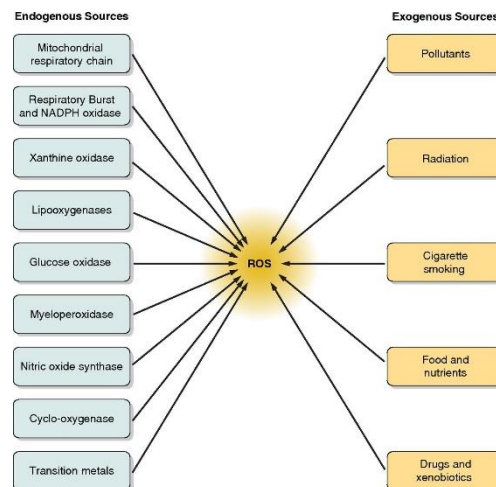
FIGURE 1 –Sources of ROS. [2]

ROS plays a role in many vital physiological processes, including phagocytosis, apoptosis, cell signaling, and wound healing [2]. However, an excess of ROS can lead to the degeneration of important biomolecules, such as nucleic acids, proteins, lipids, and carbohydrates. This excess of ROS can subsequently lead to inactivation of target molecules, cause DNA damage, and stimulate apoptosis in cells [2]. Chronic overproduction of ROS has been found to lead to the formation of many debilitating diseases, such as cancer, diabetes, atherosclerosis, rheumatoid arthritis, chronic inflammation, Parkinson's disease, Alzheimer's disease, multiple sclerosis, and amyotrophic lateral sclerosis [1].
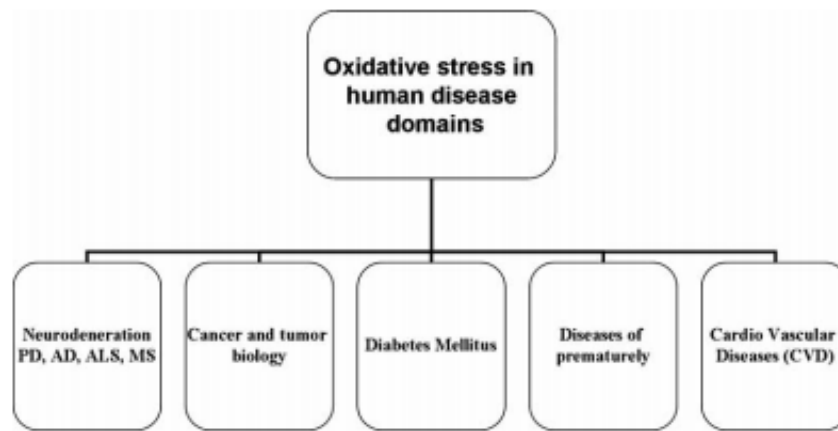
FIGURE 2 –Oxidative stress and human diseases. [1]

The body naturally eliminates ROS by utilizing ROS scavenging compounds, called antioxidants. The antioxidant defense system is the body's way of using enzymatic or non-enzymatic methods for eliminating and preventing ROS production. A type of natural enzymatic antioxidants are superoxide dismutases. One function of these enzymes is to scavenge uncharged H_2O_2 as it crosses mitochondrial membranes [2]. Thioredoxin is an important non-enzymatic antioxidant that regulates redox-sensitive proteins by

16

inhibiting ROS interactions [2]. Overall, antioxidants have the ability to oxidize or

reduce ROS, bind to ROS precursors, inhibit the formation of ROS, and bind to metal

ions that subsequently catalyze ROS formation [1][2]. Despite the presence of

endogenously formed antioxidants in the body, supplemental dietary antioxidants, such as

vitamin C, vitamin E, vitamin A, and glutathione, are essential for ROS regulation [2]. A

balance of natural and supplemental antioxidants are needed to effectively remove ROS

from the physiological system. If ROS production is unmitigated due to insufficient

antioxidant quantities, subsequent cellular and tissue damage may occur.

B. Antioxidants

1. Curcumin

    Curcumin, also called diferuloyl methane, is a pigment found in turmeric that

exhibits anti-inflammatory and antioxidant properties [3]. Clinical trials involving high

doses of curcumin has shown that it is safe, nontoxic, inexpensive, and therapeutically

effective for a variety of human diseases [3]. Such diseases include cancer,
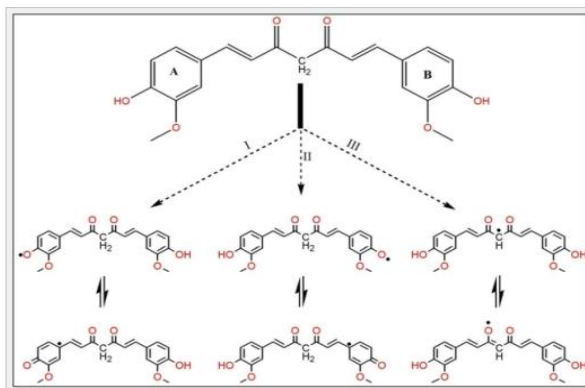
FIGURE 3 –Chemical structure of curcumin and its three pathways for scavenging ROS [4].

cardiovascular disease, arthritis, atherosclerosis, diabetes, renal conditions, Crohn's disease, and many other inflammatory diseases.

In terms of the antioxidant capabilities of curcumin, there are three potential reaction sites where curcumin can react with and eliminate ROS: a diketone (FIGURE 3 Pathway III) and two phenolic groups (FIGURE 3, Pathways I and II) [5]. As seen in FIGURE 3 I and II, ROS reacting with the phenolic groups yields a radical that can be transferred around the phenolic group, leading to radical stabilization and elimination. When ROS reacts with the carbon in between the diketone groups, like in FIGURE 3 III, a radical is formed on the center CH_2 group which can be further stabilized by transferring electrons throughout the ketone groups. Curcumin's ability to transfer electrons is due to its symmetric structure, beta-diketone, and pi electrons [4][5]. These properties of curcumin make it an extremely effective antioxidant, because it is able to stabilize free radicals and prevent them from causing damage to biomolecules and cellular components. However, despite curcumin's excellent antioxidant capabilities, its therapeutic efficacy is limited due to its own various properties: poor intestinal absorption, rapid metabolism, short biological half-life, and low oral bioavailability [3].

Curcumin has extremely poor oral bioavailability due to its poor intestinal absorption, rapid metabolism, and rapid systemic elimination [3]. Various characteristics of curcumin, such as its low water solubility and photosensitivity are thought to hinder its ability to be absorbed by the intestines [6]. Intestinal pH was found by Berginc et al to also have an effect on curcumin intestinal permeability. In rat jejunum and Transwell grown Caco-2 cells, curcumin had a slight increase in permeability under acidic conditions, though curcumin permeation was still considered very low [7]. Other factors

that limit the intestinal absorption of curcumin are the presence of various intestinal enzymes and transporters, such as P-glycoprotein and nonspecific oxydoreductases, that metabolize curcumin before reaching systemic circulation [7][6]. Curcumin also has an extremely short biological half-life, approximately 0.31 ± 0.07 hours in rats [6]. These characteristics of curcumin in physiological conditions lead to the overall poor bioavailability of curcumin, rendering this potentially powerful antioxidant essentially therapeutically ineffective.

2. n-2-mercaptoproprionyl glycine (N-MPG)

N-MPG is an aminothiol compound with the ability to scavenge ROS and decrease radiation-induced lipid peroxidation [8]. It has been proposed for treatments of various conditions, including cystinuria and protection against ischemia-reperfusion injury in hypertrophied hearts [8][9]. N-MPG is an effective antioxidant due to its free thiol group. The free thiol group is able to be oxidized to create a disulfide bridge with another N-MPG molecule, forming disulfide dimers [8]. Despite N-MPG's antioxidant capabilities, N-MPG has limited therapeutic efficacy due to its poor half-life. In physiological conditions, N-MPG only has a relative half-life of 1-2 hours [10].
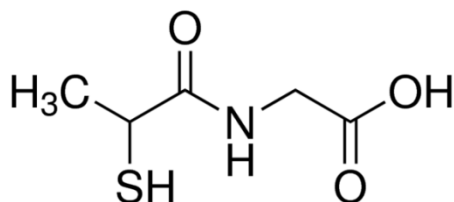
FIGURE 4 –Chemical structure of N-MPG [11]

3. Current Delivery Methods

Various alterations have been made to improve the bioavailability and stability of curcumin and N-MPG, separately. Nanoparticle formulations, such as liposomes, nano- or micro- emulsions, polymeric nanoparticles, solid lipid nanoparticles, polymer conjugates, nanocrystals, polymeric micelles, nanogels, and self-assemblies have been intensely studied for improving the therapeutic efficacy of these antioxidants, separately, by increasing bioavailability [6] [12] [13]. Most of these modifications have slightly improved the oral, injection, and transdermal methods for delivering these antioxidants. The goal of this paper is to investigate a method for delivering these antioxidants, combined, using transdermal delivery.

C. Transdermal Drug Delivery

Transdermal drug delivery is the systemic administration of therapeutic agents by penetrating them through the skin. This method of drug delivery is beneficial for therapeutic agents, such as curcumin, that are easily degraded by the gastro-intestinal tract and/or undergo the first-pass effect of the liver [14]. When orally administered, curcumin is usually degraded and unabsorbed by the small intestine, rendering oral delivery of curcumin ineffective. Transdermal delivery of curcumin will allow curcumin to reach systemic circulation without having to enter the hostile environment of the gastro-intestinal tract. Therefore, transdermal delivery of curcumin has the potential to be more therapeutically effective compared to oral drug delivery of curcumin. Another common method for administering curcumin and N-MPG is through needle injections, which are painful and require frequent needle sticks due to fast drug-clearance [14].

Needle injections also have the potential to result in wound site infection, which could subsequently lead to sepsis. It also generates dangerous medical waste and can increase risk of disease transmission if needles are improperly disposed of [15]. Due to the painfulness of the injection method of drug delivery, it also typically has low patient compliance. Transdermal delivery does not require frequent injections, allowing for a controlled and infection-free delivery of curcumin and N-MPG. Overall, transdermal delivery of curcumin and N-MPG has the potential to increase the systemic administration of these therapeutic agents in a controlled, non-invasive fashion.

The main hindrance for transdermal delivery is penetration of the agent(s) through the skin to reach dermal capillaries. Human skin is composed of three main layers: epidermis, dermis, and subcutaneous [15]. The stratum corneum is the outermost layer of the epidermis and is the main barrier to successful transdermal delivery [15]. The stratum corneum is commonly compared to a brick wall, with the bricks being the keratin-rich corneocytes and the mortar being the intercellular lipid lamella [15]. The intercellular lipid lamella is in a highly organized crystalline structure and is an essential component for the barrier properties of the stratum corneum [15]. The other layers of the epidermis (stratum lucidium, stratum granulosum, stratum spinosum, stratum basale) also provide hindrance for further permeation. Ultimately, the target layer of the skin for transdermal drug delivery is the dermis. This layer of the skin contains small capillary vessels; therefore, if the drug reaches this layer, the drug can potentially enter the capillaries and reach systemic circulation [15]. However in the dermis, capillary hydrostatic pressure, lymphatic uptake, and endothelial permeability can provide physical barriers for systemic

absorption of the drug. As a first step for transdermal delivery of curcumin and N-MPG, this work focuses on their permeation through the stratum corneum.
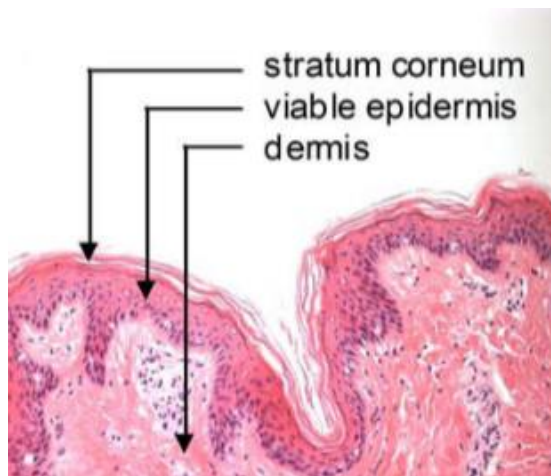
FIGURE 5 –H&E stain of skin, illustrating its layers [14].

D. Lipid Vesicles

1. Traditional Liposomes

One method to penetrate curcumin and N-MPG through the stratum corneum, utilizes lipid vesicles, or liposomes. Liposomes are essentially phospholipids that have aggregated in a lipid bilayer(s) to enclose an aqueous medium. Therefore, liposomes have the ability to contain lipophilic drugs in their lipid bilayer, such as curcumin, and hydrophilic drugs in the encapsulated aqueous medium, such as N-MPG (see FIGURE 6) [15]. Because the cell membrane of human cells is composed of a phospholipid bilayer, liposomes can be formed that are non-toxic, biodegradable, and a natural permeation enhancer [15]. The lipid composition also helps to increase the bioavailability by protecting the drug from degradation. Liposomes also have the ability to increase the

stability of the encapsulated drug, which is essential for delivering curcumin and N-MPG because of their short half-lives [6][10]. Liposomes also have the potential to provide a sustained/controlled release of the drug [15]. After skin permeation to the dermal layer, the liposome must pass through capillary endothelial cells to reach systemic circulation. During systemic circulation, the liposome will have to circumnavigate phagocytic cells to ultimately undergo endocytosis with target cells.
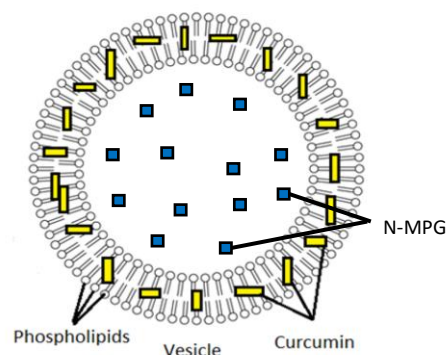
FIGURE 6- Schematic of Liposome containing curcumin and N-MPG

Over the years, modifications have been made to liposomes to increase the efficacy of their transdermal delivery. One modification was to add a non-ionic amphiphile surfactant to the composition of the vesicles, forming a new type of vesicle called niosomes [15]. These vesicles improved penetration, but not into the deeper skin tissues. However, with the development of ultradeformable liposomes and ethosomes, by Cevc et al and Touitou et al respectively, vesicle penetration through the stratum corneum and into the deeper layers of the skin improved drastically [15]. Ultradeformable liposomes are liposomes that also contain an edge activator in their lipid bilayer, while ethosomes are liposomes that are made in an ethanol/water solution.

A common method for liposomal fabrication is called the mechanical-dispersion method. This method involves dissolving the lipids in a solvent, typically chloroform. The lipids are then dried down by evaporating off the solvent. This leaves a film of lipids on the container, which is then rehydrated in a buffer solution at 37^0C for an hour. Probe sonication can then be used to break apart the lipids, causing them to aggregate into a smaller lipid vesicle. Verma et al, 2002 found that vesicle sizes of 120 nm compared to 191 nm, 377 nm, and 810 nm had more vesicle permeation through the stratum corneum and into the deeper skin layers [17]. Therefore, the main criterion established for particle fabrication was to develop particles less than 200 nm, in order to allow for particle migration through the skin during transdermal delivery [17].

2. Ultradeformable Liposomes

Ultradeformable liposomes are hydrophilic lipid vesicles composed of phospholipids and a single chain surfactant called an edge activator. The phospholipid typically used in the formation of ultradeformable liposomes are various phosphatidylcholines, either soya or egg phosphatidylcholine [15] [18]. Potential edge activators include cholic acid; span 60, 65, or 80; and tween 20, 60, or 80 [15][18]. The addition of the edge activator to the liposome composition increases the deformability of the vesicles, allowing them to squeeze through the channels in the stratum corneum [18].
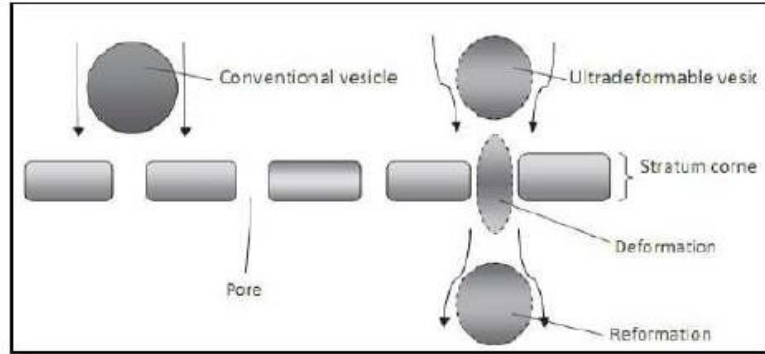
FIGURE 7 – Conventional versus Ultradeformable vesicle moving through the stratum corneum [18].

The main mechanism behind increased penetration of ultradeformable liposomes is the osmotic gradient of the skin. [15]. Dry skin at the surface of the skin is approximately 20% water, while the underlying epidermis is approximately 100% water [15][18]. This gradient drives the ultradeformable liposomes movement through the brick-walls of the stratum corneum.
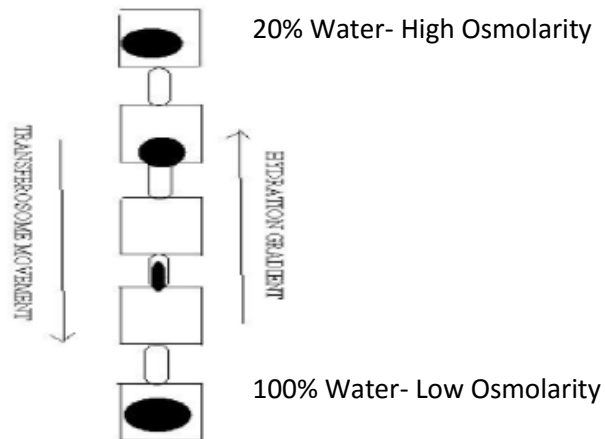
FIGURE 8 – Osmotic gradient of skin, and subsequent movement of ultradeformable liposome [15].

The main method for producing ultradeformable liposomes is the mechanical-dispersion method described under Traditional Liposomes. The only difference is that during the hydration phase of vesicle formation, the lipids are hydrated for 15 minutes at 43^0C and then placed in 2-8^0C for an hour [15]. The vesicles reach their maximum hydrodynamic radius at the colder temperature and are later reduced in size with processes such as probe sonication, freeze-thaw, and reverse evaporation [15].

3. Ethosomes

Ethosomes are lipid vesicles composed of phospholipids, a high concentration of ethanol, and water. The typical phospholipids used are either soya phosphatidylcholine (Soy-PC) or egg phosphatidylcholine. The ethanol concentration ranges from 20-45% in water. Other potential additives include a polyglycol and cholesterol to increase skin permeation and increase vesicle stability [15][19]. Typically, the ethosomes made with a higher ethanol concentration yielded smaller vesicle diameters and had increased skin permeation [15].
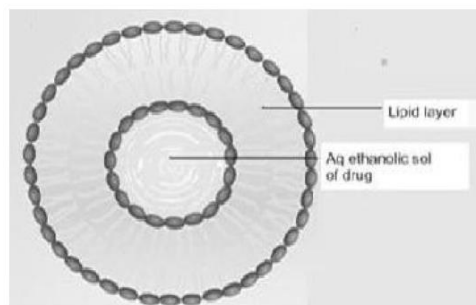
FIGURE 9 –Ethosome particle [19].

Due to the high concentration of ethanol, ethosomes typically have a very high encapsulation efficiency of hydrophilic and lipophilic molecules [15]. It also increases the fluidity of the vesicles, as well as the fluidity of the skin layers. The ethanol works to

26

solubilize the lipid lamella, creating defects in the lipid lamella the fluidic vesicles are then able to maneuver through [15][19].
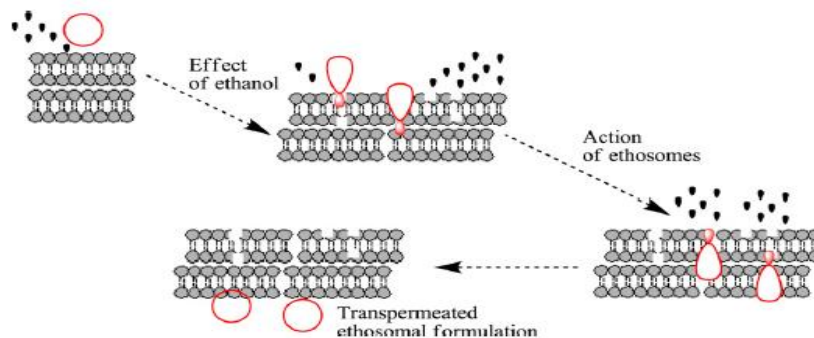
FIGURE 10 –Schematic of Ethosome movement through skin [20]

Two commonly used methods for fabricating ethosomes include the mechanical-dispersion method and the cold method. The mechanical dispersion method is similar to the process described in the Traditional Liposomes section, except ethanol is incorporated into the buffer (20-45%) [19]. The cold method involved dissolving the lipids in ethanol, heating this lipid-ethanol solution and heating water to $30^{0}C$, and then mixing the two solutions together with stirring [19]. The lipid vesicles can then be reduced in size through probe sonication.

4. Previous Study

Previously, fusogenic liposomes were developed by this group using the lipid to N-MPG to curcumin ratio 10:1:0.48 (mg/ml) for the purpose of injection delivery. Curcumin was trapped inside the lipid bilayer while N-MPG was encapsulated inside the aqueous medium of the lipid vesicle. Despite the potential of these fusogenic liposomes, the required intravenous injection of this therapy was deemed undesirable. Therefore, an alternative method for delivery of curcumin and N-MPG was sought after.

E. Hypothesis and Specific Aims

Lipid vesicles containing the antioxidants curcumin and N-MPG can be modified to permeate these therapeutic agents passed the stratum corneum of the skin. To address this hypothesis, these aims were specified:

1. Fabrication of traditional liposomes, ultradeformable liposomes, and ethosomes containing the antioxidants curcumin and N-MPG that are less than 200 nm in diameter.

2. Characterization of each vesicle for stability, morphology, and entrapment efficiency in order to compare vesicle types.

3. Investigation of the transdermal delivery potential of each type of vesicle using pig skin.

II. METHODS

A. Vesicle Fabrication

Using the fusogenic liposomal compositions previously developed by our group, the composition of the traditional liposomes was 10 mg/ml Soy-PC, 1 mg/ml N-MPG, and 0.48 mg/ml curcumin, in a PBS solution. The Soy-PC, specifically Phospholipon 90G (Lipoid, Ludwigshafen, Germany), contains 95% soy-phosphatidylcholine, 2% lyso-phosphatidylcholine, 2% fatty acids, and other lipid soluble substances (See FIGURE 11) [21]. The traditional liposomes were fabricated using the mechanical-dispersion method. In this method, 250 mg of Soy-PC (95%) was dissolved in 1 ml of chloroform and 200 µl of this solution was added to a test tube. Next, 50 mg of curcumin (Sabinsa) was dissolved in 2.5 ml of acetone and 120 µl of this solution was added to the test tube. The solvents were then evaporated off using a steady stream of nitrogen gas, leaving a lipid residue. The lipid residue, or thin film, was then placed under vacuum (Thermo, Air Cadet) for 24 hours in order to completely remove any remaining solvents.

FIGURE 11 –Chemical structure of Soy-PC [21]

The lipid residue was then rehydrated by adding 5 ml of a 1 mg/ml N-MPG in PBS solution with a pH of 7.4. Two 5 mm glass beads (Sigma) were added to the test tube and it was covered with parafilm. The tube was then vortexed for 15 seconds and placed in a 37°C water bath for one hour, being vortexed every 15 minutes for 15

seconds. The contents of the tube are then removed and placed in a 15 ml centrifuge tube

for probe sonication (Branson, Sonifer 450). Probe sonication was performed with a

booster horn and micro-tip probe using a duty cycle of 60% and an output control of 7,

for five minutes. During sonication, the samples were placed in an ice water bath (16°C-

18°C) with the probe placed in the middle of the centrifuge tube and far down to where

the centrifuge tube begins to become conical. The solution was then centrifuged with a

Beckman TJ-6 at the max speed of 10,000 rpm to remove titanium particles form the

sonicator tip. The supernatant was then removed for particle size analysis using a Protein

Solutions DynaPro DLS (Wyatt Instruments, Santa Barbara, CA). Samples were stored at

4°C and protected from light.

The ultradeformable liposomes composition was determined to be 10 mg/ml Soy-

PC, 1 mg/ml N-MPG, 0.48 mg/ml curcumin, and 1.5 mg/ml cholic acid (Sigma), in a

PBS solution [22]. Patel et al similarly developed curcumin loaded transfersomes,

suggesting a lipid to span 80 ratio of 85:15 (in mmol) for optimal skin permeability of

curcumin [22]. Span 80, tween 20, and tween 80 were initially attempted for

ultradeformable liposome fabrication using that lipid to edge activator ratio. Cholic Acid

was ultimately chosen because compared to the previously mentioned edge activators, it

created a thin film of lipids, curcumin, and edge activator during fabrication.

For the fabrication of the ultradeformable liposomes, the mechanical-dispersion

methods previously described to make the traditional liposomes was utilized with slight

modifications. During the drying down phase, 167μL of a 45 mg/ml cholic acid (45 mg

cholic acid dissolved in 1 mL EtOH) was added to the test tube with the Soy-PC and

curcumin. The solvents were evaporated and the resulting lipid residue was placed under

30

vacuum, like previously described. During the hydration phase, instead of placing the test tube in a 37^0C water bath for one hour, it was placed in a 43^0C water bath for 15 minutes and then a 2-8^0C refrigerator for 1 hour. The tube was vortexed for 15 seconds every 15 minutes. The sonication, centrifugation, sonication, DLS and storage parameters remained the same as those described for the traditional liposomes fabrication.

For the ethosomes, the initial fabrication technique utilized was the mechanical-dispersion method described to make the traditional liposomes. The only difference was the lipid residue was hydrated in an ethanol solution. To determine what ethanol concentration would yield an appropriate vesicle diameter less than 200 nm, 1 mg/ml Soy-PC ethosomes in 15%, 30%, 45%, and 70% ethanol solutions were fabricated. A 40% ethanol solution containing 16.24 mg/ml of Hank's Balanced Salt Solution (HBSS) (Sigma, St. Louis, MO) and 1.33 mg/ml of Trizma base (Sigma) was chosen for future ethosome studies. The Soy-PC concentration was increased to 10 mg/ml so the ethosomes could be directly compared to the other liposome configurations. The probe sonicator duty cycle, or the length of each sonication pulse, was varied between 90%, 75%, and 60% duty cycle to determine which setting would yield a smaller vesicle diameter. The 60% duty cycle was found to yield the smaller vesicle diameter. Next, the cold method for ethosome fabrication was tested and found to yield smaller particle sizes compared to those made using the mechanical-dispersion methods. Finally, particles were sterile filtered (0.2 µm) after fabrication, yielding particles with a diameter less than 200 nm.

Thus for characterization and transdermal studies, the fabrication method used was the cold method with sterile filtering. For the cold method, 50 mg of Soy-PC

(Lipoid) and 2.4 mg of curcumin were dissolved in 2 ml of ethanol in a closed container, with stirring. This container was then heated up to 30°C for 15 minutes in a water bath. Another solution containing 16.24 mg/ml of HBSS (Sigma) and 1.33 mg/ml of Trizma base (Sigma) was also heated up to 30°C for 15 minutes in a water bath. Three ml of the HBSS and Trizma base solution and 5 mg of N-MPG were added to the Soy PC, curcumin, and ethanol solution. This combination was then stirred for 5 minutes and placed in a 15 ml centrifuge tube. The pH of the solution was adjusted to 7.4. The sample was sonicated (Branson, Sonifer 450) and centrifuged (Beckman TJ-6) using the same settings as those used for the traditional and ultradeformable liposomes. The supernatant was removed carefully and then sterile filtered through a 0.2 µm syringe sterile filter into a 15 ml centrifuge tube. The size of the particles were then analyzed using DLS. The samples were then stored at 4°C and protected from light.

Dynamic Light Scattering (DLS) analysis was used to ensure the particle sizes were less than 200 nm (n=6 per vesicle type. The software package utilized with the DLS was Dynamics V6. A model for globular proteins was used to model the particle type, and based on the autocorrelation of the intensity during measurement which can be used to determine the radius of the particles [23]. The solvent setting used to analyze the traditional and ultradeformable liposomes was PBS, while the solvent setting used for the ethosomes was 20% Ethanol. Fifty readings were taken for each sample immediately after the sample was made. The fifty diameter and polydispersity readings were averaged. The means and standard deviations of these averages were recorded. Polydispersity index is measure indicating how heterogeneous the sample is. An ANOVA post hoc Tukey test (α=0.05) was ran to determine which particle types were statistically similar in size and

polydispersity. Minitab 17 was the software used for all statistical analysis performed in this paper.

B. Liposome Stability

1. Lipid Peroxidation

The stability of each particle type, without curcumin and N-MPG, was analyzed using a PeroxiDetect Kit (Sigma). This kit was used to measure the amount of lipid hydroperoxides, which form from the oxidation of unsaturated fatty acids. First, a 90% methanol stock solution was created by combining 108 mL methanol and 12 mL water. The Organic Peroxide Color Reagent was made by adding 120 mL of the 90% methanol to the kit bottle. To make the Working Color Reagent, a ratio of 100 volumes of Organic Peroxide Color Reagent stock to one volume of Ferrous Ammonium Sulfate Reagent was added together. Next, 100 μL of the particle sample being tested was added to a 1.5 mL cuvette. Then 1 mL of Working Color Reagent was added to the cuvette. The samples were incubated at room temperature for 30 minutes, protected from light. The absorbance of the samples was measured with a spectrophotometer (Thermo) at 560nm. A standard curve plotting lipid hydroperoxides from 0 to 16 nano-moles versus their respective absorbance was created using tert-butyl hydroperoxide as a positive control without lipids. This yielded the equation $y=0.0408x + 0.0011$ with y equaling absorbance and x equaling nano-moles of lipid hydroperoxides. The $r^2=0.9976$. It was predetermined that the maximum amount of lipid hydroperoxides was 10 nmoles. The PeroxiDetect Kit was performed on each particle type at days 0, 3, 7, and 113 post-fabrication. Three samples from each particle type was assayed three times. The total mean absorbance and standard

33

deviation was used to calculate the mean nano-moles of lipid hydroperoxides and standard deviation of each particle type. A one-way ANOVA with α=0.05 was used to determine which particle type minimizes the amount of nano-moles of lipid hydroperoxides over time. Equal variance was tested prior to running the ANOVA. If equal variance could be assumed then a Tukey comparison was ran. Otherwise, a Games-Howell comparison was ran.

2. Size Analysis

The stability of each particle type, with curcumin and N-MPG, (n=6) was also analyzed by taking size measurements using DLS analysis at various time points post-fabrication [24]. Time measurements include day 0, 3, 7, 14, and 30, post fabrication as these days would likely show liposome aggregation or liposome destruction via lipid peroxidation. The particle type was determined unstable once the mean particle size was statistically different from day 0 or once the mean particle size had changed a predetermined percentage. A one-way ANOVA post hoc Tukey (α=0.05) was used to determine if particle size at each time point differed significantly from day 0. The other metric for determining particle stability involved taking the 50 measurements from each particle batch at day 0 and finding the mean and standard deviation for that sample. The standard deviation percentage of the mean was then found by dividing the standard deviation by the mean and multiplying by 100. This was then averaged for ethosomes, traditional liposomes (n=6 for both), or ultradeformable liposomes (n=4) to yield the criteria for allowable percent change in size. For ethosomes, ultradeformable liposomes, and traditional liposomes, the allowable percent change is 34.5%, 22.5 %, and 32.8%, respectively. The percent change in mean particle size from day 0 was found by taking

34

the mean particle size at day X subtracted by the mean particle size at day 0, divided by

mean particle size at day 0, and multiplied by 100.

C. Liposome Characterization Using SEM

Scanning Electron Microscopy (SEM) was used to examine the shape and size of the

liposome formulations. In order to visualize the liposomes, 15 µL of the sample was

pipetted onto carbon tape on a copper stub and left to dry for over 12 hours. The samples

were sputter coated with gold/palladium in a 0.1 torr vacuum with a voltage of 1.8 kV for

two minutes. A Zeiss Supra 35VP scanning electron microscope using a secondary

electron detector with an EHT value ranging from 1.50 kV to 3.00 kV was used to

visualize each particle type.

D. Entrapment Efficiency

The entrapment efficiency of curcumin for each lipid vesicle type was determined

using the ultracentrifugation method [25]. A Beckman L8-70M Ultracentrifuge with a

50.4 TI rotor was used to spin down three 1 mL aliquots of each sample (n=3) for 30

minutes at 40,000 rpm. Once finished, the supernatant of each sample was removed. The

supernatant was diluted in PBS, using a 50 to 950 sample to PBS volumetric ratio. A

spectrophotometer (Thermo) read the absorbance at a fixed wavelength of 425 nm. Two

concentration curves were created to determine the amount of curcumin in the

supernatants of the samples. The first concentration curve initially dissolved curcumin in

100% methanol to create a 1 mg/ml solution, because curcumin is extremely insoluble in

water. In order to mimic the solutions used to fabricate the traditional and

ultradeformable liposomes, subsequent dilutions were performed with a 1 mg/ml N-MPG

in PBS solution. This first concentration curve was graphed from 25 μM to 1000 μM of

curcumin, yielding the equation y=0.003x – 0.0726, r^2=0.9771, with y equal to

absorbance and x equal to curcumin concentration. This was then used to determine the

amount of curcumin in the supernatants of the traditional liposome and ultradeformable

lipsome samples. The second concentration curve was created by dissolving and diluting

curcumin in 40% EtOH, in order to mimic the solution of the ethosomes. This second

concentration curve was graphed from 25 μM to 400 μM of curcumin, yielding the

equation y=0.0038x + 0.1802, r^2=0.9958 with y equal to absorbance and x equal to

curcumin concentration. This equation was then used to determine the amount of

curcumin in the supernatant of the ethosome samples. Entrapment efficiency was then

calculated as a percent using the equation [25]:

$$\% \, Entrapment \, = \frac{CCMfab - CCMsupernatant}{CCMfab} \times 100$$

The percent entrapment calculations from the three aliquot readings from each individual

particle batch were averaged together. A one-way ANOVA post hoc Tukey test (α=0.05)

was then used to determine if particle type significantly affected entrapment efficiency

and if so, which type had the highest.

　　　　A typical method for quantifying the amount of N-MPG in a solution is by using

Ellman's Reagent to bind to N-MPG's free thiol group. Once bound, TNB is released and

ionizes to TNB^{2-} in water. TNB^{2-} is a yellow color and can be read at a wavelength of 412

nm on a spectrophotometer. However, this reading is masked by curcumin because it

reads at a wavelength of approximately 425 nm. Therefore, the entrapment efficiency of

N-MPG by each vesicle type was theoretically calculated using the equation in FIGURE 12.

$$EE\% = \frac{V_{in}}{V} \times 100\% = \frac{\sum_i \left(\frac{4}{3}\pi(r_i - d)^3 \cdot \frac{c \cdot V \cdot N_A}{\sum_i \left(\frac{4\pi[r_i^2 + (r_i - d)^2] \cdot P_i}{a} \right)} \cdot P_i \right)}{V} \times 100\%$$

$$EE\% \propto c, r, a, -d$$
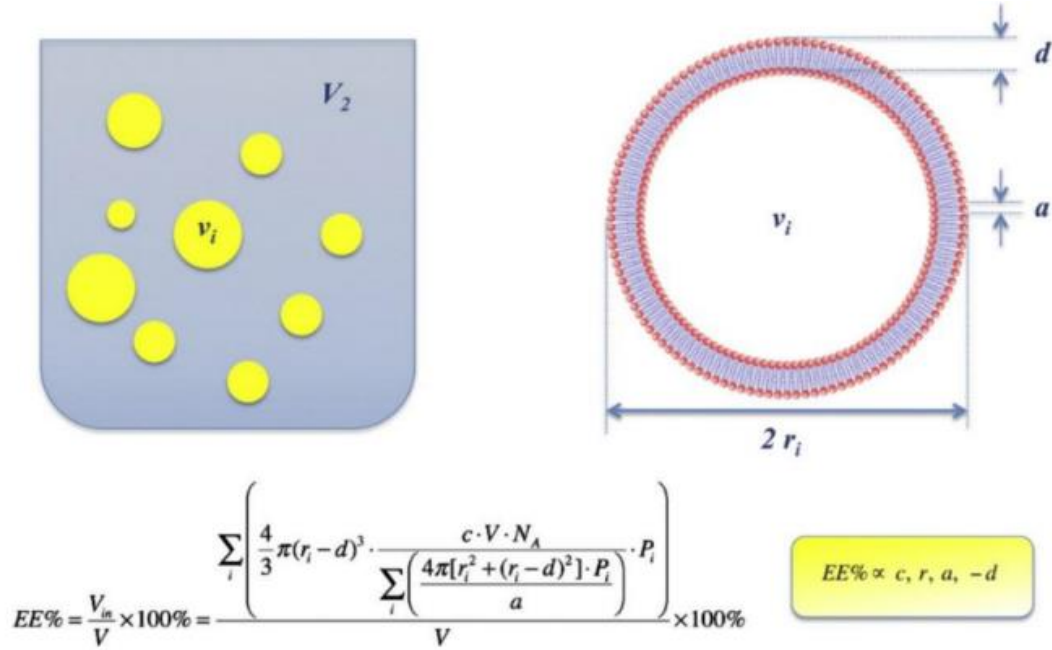
FIGURE 12 –Schematic of Theoretical Entrapment Efficiency [26]

The entrapment efficiency is a percentage of the inner volume of the vesicle (V_{in}) over the total volume of the sample (V) [26]. Inner volume is a function of the radius of the particle (r_{in}), the bilayer thickness (d), the lipid concentration (c), the amount of lipid molecules per vesicle (N_A), and the exposed area of a single lipid molecule (a). The calculation is repeated with probability weights (P_i) over a log normal distribution of vesicle sizes [26]. For each particle type, the bilayer thickness (d) was assumed to be 4.9 nm [26], the mean molecular area of a single lipid molecule (a) was assumed to be 40 Å [26], the lipid concentration (c) of the sample was 10 mg/ml or 12.9 mM, and sample volume (V) was 5 mL. The particle size and size distribution of each particle type was

chosen to be the diameter and standard deviation reported in the "Vesicle Fabrication" section of the results.

E. Skin Permeation

In order to determine if the lipid vesicles were able to penetrate into the dermis layer of skin, testing was performed using pig skin and a modified Franz diffusion chamber [26]. The pig skin came from the abdominal region of one year old Yucatan or Yorkshire pigs immediately after they were sacrificed. Upon excision, the skin was washed with 7.4 pH PBS and stored at 4^0C for a maximum of two days. Fat and muscle layers were removed from the skin layers using a scalpel.
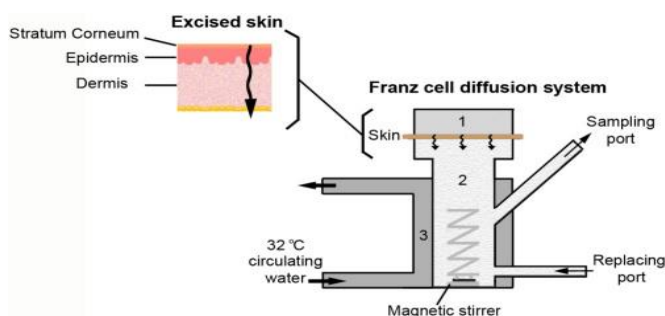
FIGURE 13 – Franz Diffusion Chamber [27]

A Franz Diffusion Chamber is an apparatus that allows one to determine the pharmacokinetics of a transdermal treatments. The typical Franz Diffusion Chamber can be viewed in FIGURE 13. Compartment 1 is the donor compartment that houses the treatment being tested [27]. Below this compartment is where the skin is placed. Compartment 2 houses a warm circulating solution where the sample will travel once it has migrated through the skin [27]. The traditional Franz Diffusion Chamber was recreated using a 12 cell well plate and its respective cell culture insert (FIGURE 14).
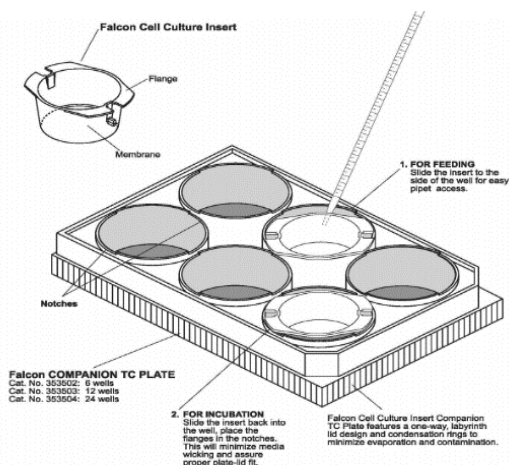
FIGURE 14 -12 cell well plate and insert used for modified Franz Diffusion Chamber [28].

The excised skin was cut into circular pieces using a metal cylinder approximately 10 mm in diameter. The circular skin pieces were then placed into the 12 cell well cell culture insert with the dermis layer facing downward. The skin was fastened and sealed to the cell culture insert by placing 20 μL of surgical glue (Vetbond Tissue Adhesive) around the edges of the skin. Once the glue dried, 1.25 mL of the vesicle treatment was placed on top of the skin. The cell inserts were placed on white paper for 5 minutes and analyzed for leakage before being used. A stir bar and 700 μL of PBS-Ascorbic Acid (100 μL of 1M ascorbic acid/2.9 mL PBS) were placed into each cell well. Then, the skin cell culture insert with treatment was added to the cell well. Once a 12 cell well plate was filled with skin cell culture inserts, the top was secured and the cell plate was wrapped in parafilm and aluminum foil. It was then placed in a 37^0C room on top of a stir plate.
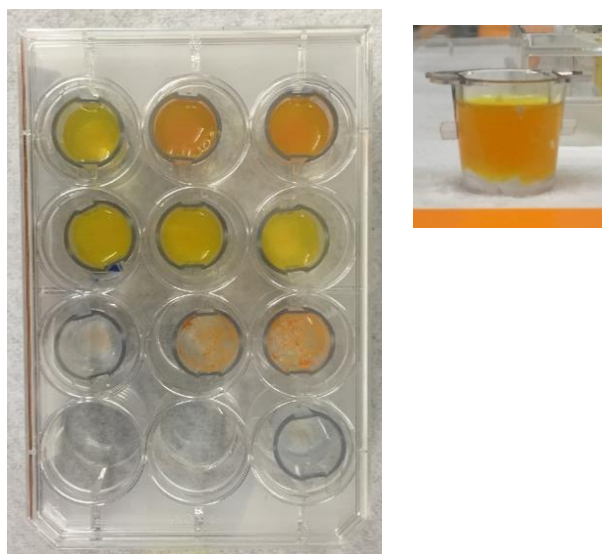
FIGURE 15 –Image of cell well insert with skin and treatment, in the 12 cell well plate.

The skin permeation of the three liposome formulations was examined over a 24 hour time period. A Thermoscientific NanoDrop 2000c Spectrophotometer was used to take absorbance measurements of the solution in the lower chamber at hours 2, 8, 18, and 24. Control treatments include PBS and free curcumin in PBS, while liposome treatments include drug-loaded ethosomes, ultradeformable liposomes, and traditional liposomes. Each treatment had a skin-containing cell insert with an n=2. Three absorbance readings were taken from each cell well by placing 2 µL of the sample onto the NanoDrop reader. However, the use of the NanoDrop Spectrophotometer was deemed not sensitive enough to detect the curcumin that permeated the skin.

The skin permeation study was replicated, taking fluorescence measurements using a fluorometer, (Turner) instead of taking absorbance measurements using the NanoDrop. A fluorometer was thought to detect lower concentrations of curcumin

compared to the NanoDrop. A Turner Biosystems Modulus with the Blue LED (465 nm to 485 nm wavelength) was used to measure Fluorescent Specific Units of the solution contained in the cell well. 125 µL of the sample was placed in glass microtube and read. The time points for this study were hours 2, 7, 17, 24, and 41. However, this measure was also determined not sensitive enough.

Since utilizing the NanoDrop and fluorometer were determined to be ineffective in measuring lipid vesicle permeation, another measure determining amount of lipid vesicles deposited in the skin was performed. In this testing, the modified Franz Diffusion Chamber was set up like previously described. Treatments performed were a PBS control (n=3) and each lipid vesicle formulation (ethosomes: n=4; ultradeformable and traditional liposomes: n=3). After 24 hours in the modified Franz Diffusion Chamber, the Yorkshire pig skin sections were removed from cell culture inserts with a scalpel and placed in 2 mL centrifuge tube with 1 mL of 200 proof EtOH to extract curcumin deposited in the skin. The centrifuge tubes were then placed in an ultrasonic bath (Fisher Scientific FS60) for 1 hr [29]. Three fluorescence readings were then taken from each sample using the Turner Biosystems fluorometer. Skin deposition was also determined at hour 2(PBS: n=3; ethosomes: n=4; ultradeformable and traditional liposomes: n=3). A one-way ANOVA post hoc Tukey (α=0.05) was used to determine if treatment affected skin deposition and to compare treatments.

The Yorkshire pig skin from the skin permeation study involving the NanoDrop reader was post-processed. The skin was removed from the cell culture insert with a scalpel and then placed in 4% formaldehyde for 48 hours. Next, the skin was placed into a 30% sucrose solution for a minimum of 48 hours or until the tissue sank to the bottom

of its container. Then, the tissue was embedded in a tissue mold (Peel-A-Way ®) by freezing the tissue in optimal cutting temperature (Tissue-Tek ®) compound using dry ice. Once frozen, the tissue block was covered in aluminum foil and stored at -80^{0}C. A cryotome (Thermo Electron Corporation Shandon FSE), with the cryobar -50^{0}C, the chamber -20^{0}C, and the specimen -20^{0}C, cut the blocks of tissue into 30 μm sections. Once cut, the sections were placed onto microscope slides. Slides from each treatment type was used for imaging the curcumin fluorescence in the skin and for histological staining of the skin.

A hematoxylin and eosin stain (H&E) was performed on the cut skin samples in order to differentiate the skin layers. First, the microscope slides were heated on a hot plate at 65^{0}C for 20 minutes. Then the tissue was hydrated in DI water for 2 minutes, two times. The slides were then placed in 0.1% Hematoxylin (Sigma) for 10 minutes. Then the sections were washed with tap water three times, each for 1 minute. The microscope slides were then dipped in 0.5% Eosin Y in 95% EtOH (Sigma) for 15 seconds. The eosin was then washed off twice with DI water. The tissue was dehydrated by placing the slides in increasing ethanol concentrations: 50%, 70%, 95%, and100%. The microscope slides were placed in each ethanol solution for two minutes, two times. Then the slides were placed in xylene for 1 minute before a coverslip was attached with Permount [30]. The H&E stained slides were then imaged with a digital inverted microscope (Evos xL Core, Waltham, MA) using a magnification of 40x, a brightness of 84, and a cool color balance. Three pictures were taken for each treatment. The images were then loaded into the NIS Elements program in order to measure two lengths: the top of skin to the bottom of stratum corneum and the bottom of stratum corneum to the bottom of epidermis. Three

length measurements were taken for each skin layer in each image by measuring from the two outer edges and the middle of the skin (see FIGURE 16). These length measurements were used for fluorescent image analysis.
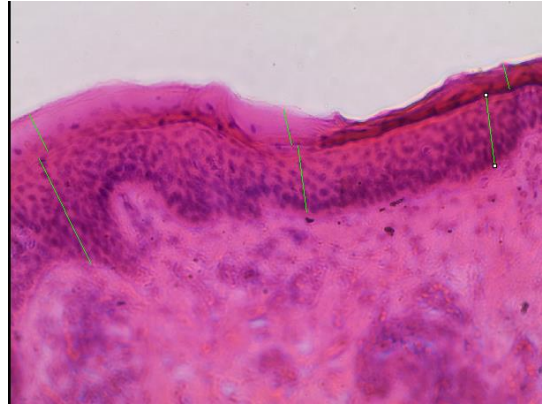
FIGURE 16 –Example image of length measurements taken of H&E stained tissue.

A confocal microscope (Nikon Eclipse Ti) was used to capture fluorescent images of the cut skin tissue using NIS Elements software. Since curcumin naturally fluoresces green when exposed to blue light, any curcumin or curcumin containing particle can be visualized using fluorescent microscopy. Appropriate sections were found using the bright field setting. The light source was switched to green fluorescent protein (GFP) with an excitation wavelength of 488 nm. The control PBS treated skin had brightness and color automatically adjusted to minimize auto-fluorescence of the tissue. These settings were then used to image the remainder of the skin treatments. All pictures were taken on 60x magnification. Three images, bright field and GFP, were taken per treatment.

To analyze the fluorescent images, the skin layer lengths determined from the H&E stain were used. Three boxes, each a 35 X 35 μpixels, were drawn per skin layer per image. They were randomly placed in each skin layer by using the lengths found from the H&E stain. Another box was drawn outside of the skin to determine background noise. The boxes were then analyzed to find the sum intensity of each box. The sum intensity of the background box was subtracted from the other box measurements taken from that image to remove the noise. This was done for each treatment: PBS, free curcumin in PBS (control treatment), ethosomes, ultradeformable liposomes, and traditional liposomes. The sum intensity from the PBS condition was averaged for each skin layer. These averages were then subtracted from the sum intensities found for the other treatments in order to remove natural skin fluorescence from their measurements. Therefore, any excess fluorescence found in the skin layers is from the curcumin in the treatments. A one-way ANOVA post hoc Tukey (α=0.05) was performed for each skin layer-- stratum corneum, epidermis, and dermis-- to determine if treatment affects Sum Intensity and if so, which treatment corresponds to the highest fluorescence in the skin layer.
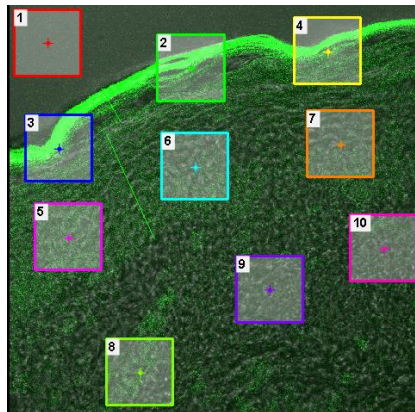

FIGURE 17 –Example image of Sum Intensity measurement.

III. RESULTS

A. Vesicle Fabrication

In order to fabricate the traditional liposomes, the common mechanical-dispersion method was chosen for its ease of use. Soy-PC was utilized as the bilayer forming lipid in all particle formulations because it is commonly used in the development of ultradeformable liposomes and ethosomes [15][18]. This lipid and the concentration of 10 mg/ml Soy-PC was kept consistent across all particle types, so the additives that caused varying particle characteristics could be pinpointed.

The mechanical-dispersion method was utilized during the fabrication of the ultradeformable liposomes. Initially, the ultradeformable liposomes were made using span 80 as the edge activator. However, during the drying down phase of fabrication, the solvent of the span 80 would not evaporate, yielding a viscous solution containing trace amounts of chloroform and acetone. Tween 20 and tween 80 were also attempted to be used as an edge activator yielding similar results. Therefore, the lipid residue could not be created with these surfactants, preventing further fabrication. Cholic acid was then tried with successful results, rendering it the edge activator of choice.

The original method used for ethosome fabrication was the mechanical dispersion method. The concentration of ethanol to be used for the hydrating solution was tested by making the particles in various ethanol concentrations. A high ethanol concentration is desired, because it typically leads to increased skin permeation [19]. For these trials, a lipid concentration of 1 mg/ml Soy-PC was utilized because only the trends were sought after.
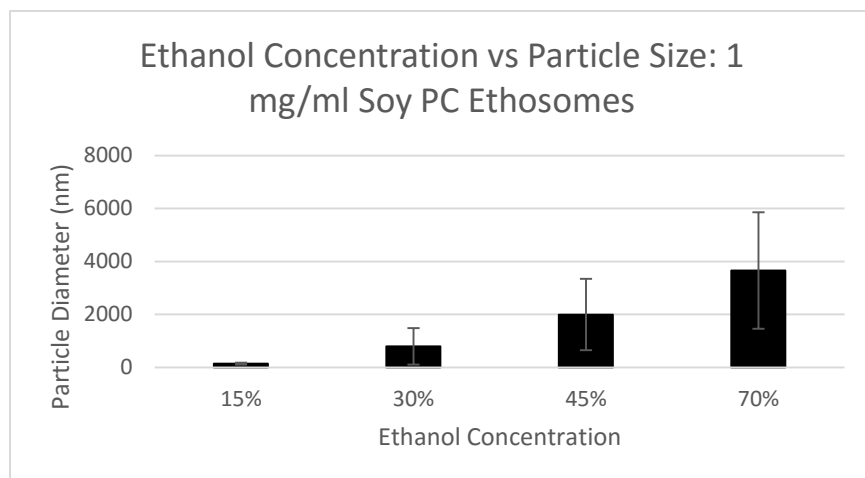
FIGURE 18 – Effect of ethanol concentration on size of ethosomes (n=1)

Contrary to literature findings, the higher ethanol concentrations yielded larger vesicle diameters [19]. Therefore, in order to decrease the vesicle diameter and still maintain a high ethanol concentration, a 40% ethanol, 16.24 mg/ml HBSS (Sigma), and 1.33 mg/ml Trizma base (Sigma) solution was chosen to make future ethosomes. The HBSS and Trizma base were added to the ethanol solution as buffers.

Since the size of the ethosomes remained greater than 200 nm, the sonication duty cycle was varied to determine the optimal duty cycle setting. The duty cycle determines the length of each sonication pulse. Sonication introduces a high amount of sound energy into the solution, causing the lipids to rearrange into smaller vesicles. However, this high energy can also cause the generation of lipid hydroperoxides, leading to instability and ultimate degradation of the vesicles. The desired duty cycle setting is low, while still creating small vesicle sizes. The sonication duty cycle chosen was 60%, because it was lower and yielded particle sizes comparable to the 75% and 90% duty cycles.
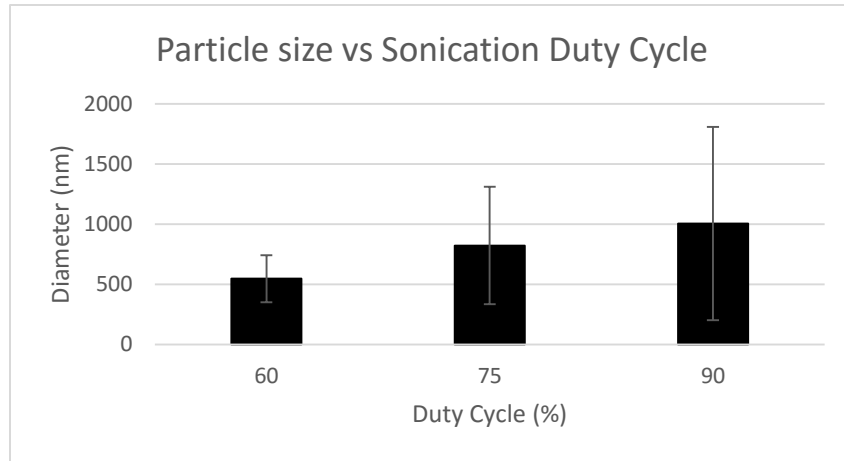
FIGURE 19 –Effect of probe sonicator duty cycle on ethosome size (n=1)

Next, the cold method for ethosome fabrication was attempted to lower particle size. After running the particles through a 0.2 µm syringe sterile filter, the particles decreased to a diameter below 200 nm. Therefore, the cold method, 40% ethanol, a duty cycle of 60%, and a sterile filter were used for ethosome fabrication for all subsequent studies. These parameters were only examined with the ethosomes because the vesicle types were inherently less than 200 nm, unlike the ethosomes.

FIGURE 20 –Effect of fabrication technique on ethosome size n=1. Graphed with standard error of mean.

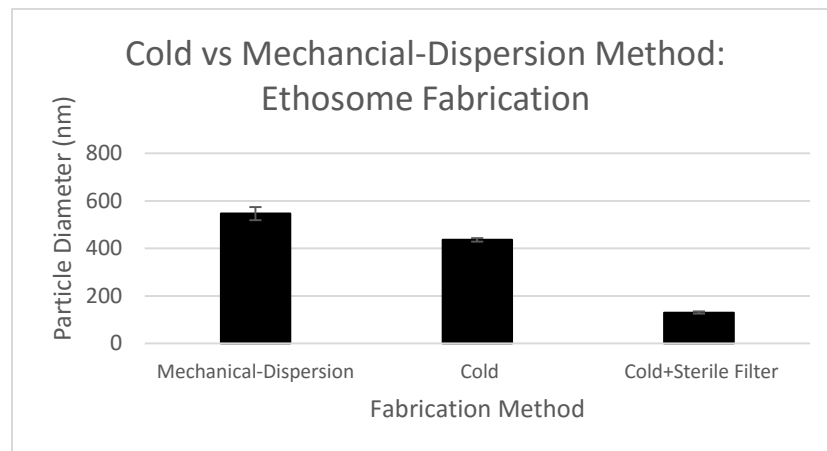Ideal particle sizes are less than 200 nm for vesicle skin permeation [17]. In order to ensure particle sizes were below this value, DLS analysis was performed on each particle type (n=6). Fifty measurements were performed for each reading. Size measurements and polydispersity are reported in TABLE 1. Liposome type was found to statistically affect particle size (p=0.015) and polydispersity (p=0.030). The ethosomes and ultradeformable liposomes were found to be statistically different in particle size (p=0.012) while the ethosomes and traditional liposomes were statistically different in polydispersity (p=0.028).

TABLE I

MEAN PARTICLE DIAMETER AND POLYDISPERSITY

Particle Type	Diameter mean (nm) ± standard deviation (nm)	Polydispersity mean (%) ± standard deviation (%)
Traditional Liposomes	127.43 ± 16.22	47.92 ± 10.84*
Ultradeformable Liposomes	81.63 ± 18.22*	55.93 ± 24.06
Ethosomes	106.50 ± 33.17*	75.70 ± 11.17*

 *denotes statistically different.

In conclusion, all vesicle types were made with 10 mg/ml Soy PC, 0.48 mg/ml curcumin, and 1 mg/ml N-MPG. The traditional liposomes and ultradeformable liposomes were made using the mechanical-dispersion method. The ultradeformable liposomes also contained 1.5 mg/ml cholic acid. These two particle types were easily less than 200 nm in size. In order to make the ethosomes less than 200 nm in size, they had to

be fabricated using the cold method, 40% ethanol, a sonication duty cycle of 60%, and sterile filtered.

<div align="center">B. Liposome Stability</div>

1. Lipid Peroxidation

The lipid peroxidation of the non-drug loaded particles was analyzed using a PeroxiDetect Kit (Sigma) (FIGURE 21). This kit detects the amount of lipid hydroperoxides in a sample. Once lipid hydroperoxides form, they propagate throughout the sample causing the lipid vesicles to degrade. The antioxidants in the drug-loaded particles can quench lipid hydroperoxides; however, this limits their therapeutic effectiveness. Therefore, understanding when the lipid hydroperoxides start to form is important for determining vesicle stability and efficacy. The PeroxiDetect Assay was performed on days 0, 3, 7, and 113 on each vesicle type. Three samples from each particle type was assayed three times.

A one-way ANOVA post hoc Tukey test ($\alpha=0.05$) was performed to determine which particle type minimizes lipid hydroperoxide formation at each day. Equal variance could be assumed for days 0, 3, and 7. At days 0, 3, and 7, particle type was found to statistically affect amount of lipid hydroperoxides, with p values equal to 0.000, 0.000, and 0.001 respectively. At days 0 and 3, all three liposomes were statistically different, with the ethosomes containing the least hydroperoxides (Day 0: $p<0.003$, Day 3: $p<0.008$) and the ultradeformable liposomes containing the most (Day 0: $p<0.003$, Day 3: $p<0.001$). At day 7, the ethosomes and traditional liposomes were statistically similar ($p=0.282$) and had the minimal amount of lipid hydroperoxides ($p<0.005$). At day 113,

<div align="center">49</div>

the one-way ANOVA showed that all three particle types were statistically similar (p=0.518).

To determine which days are significantly different in lipid hydroperoxide amount after initial post-fabrication, a one-way ANOVA with α=0.05 was performed on each particle type. This showed that days statistically affected lipid hydroperoxide amount for ethosomes, ultradeformable liposomes, and traditional liposomes (p= 0.000 for each vesicle type). Equal variance could not be assumed for the ethosomes and traditional liposomes. For the ethosomes, each day was statistically different with day 0 having the minimal amount of lipid hydroperoxides (p<0.025). In the traditional liposomes, day 3 had the minimal amount of lipid hydroperoxides (p<0.028), followed by statistically similar days 0 and 7 (p>0.999). Equal variance was assumed for the ultradeformable liposomes (p= 0.546). Day 3 had minimal lipid hydroperoxides (p<0.020) followed by day 0 (p<0.020).
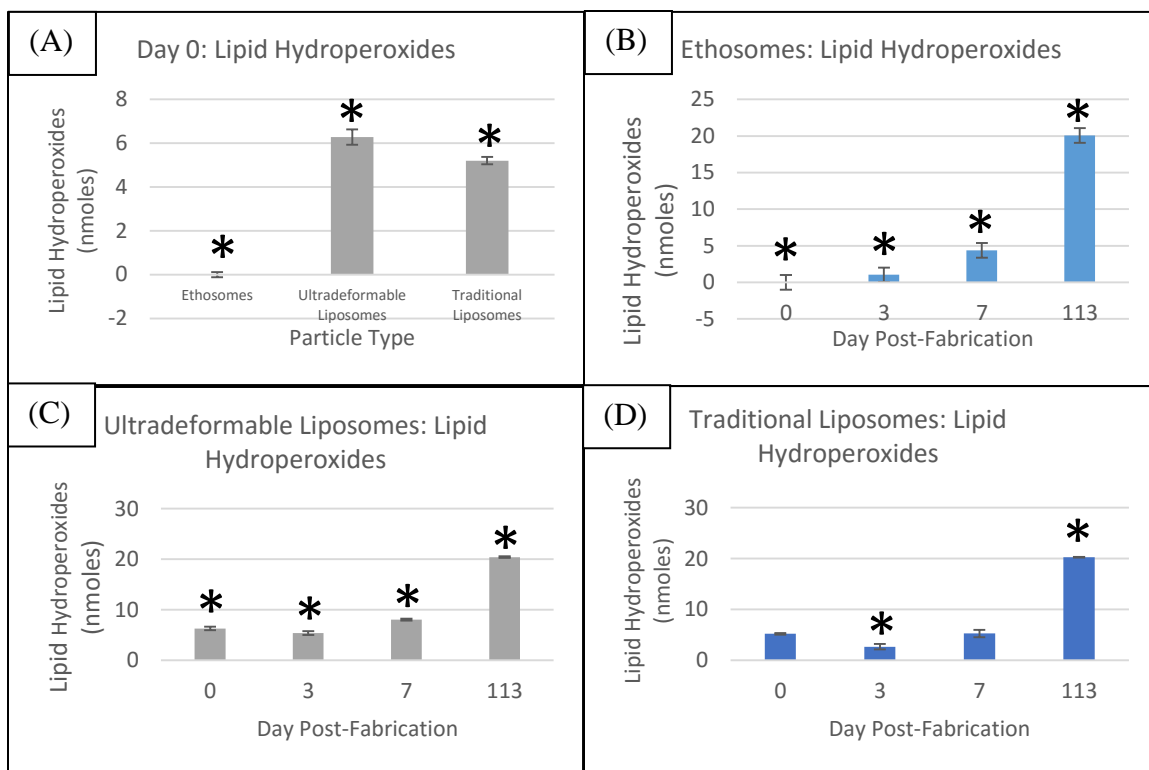
FIGURE 21 – Amount of Lipid Hydroperoxides for liposome at day 0 (A). Amount of Lipid Hydroperoxides at days post-fabrication for Ethosomes (B), Ultradeformable Liposomes (C), and Traditional Liposomes (D). * denotes statistically different.

2. Size Analysis

In order to determine the stability of the drug-loaded vesicles, the change in particle diameter was analyzed over various time points using a one-way ANOVA (α=0.05) and using a predetermined allowable change in size percentage from day 0. The ANOVA found that particle size was not statistically significant between the differing time points for the ethosomes (p=0.062) and ultradeformable liposomes (p=0.402). However, post-fabrication day was found to be statistically significant for the traditional liposomes (p=0.000); days 0 and 3 are statistically different from days 7, 14, and 30 (p<0.009 and p<0.001).
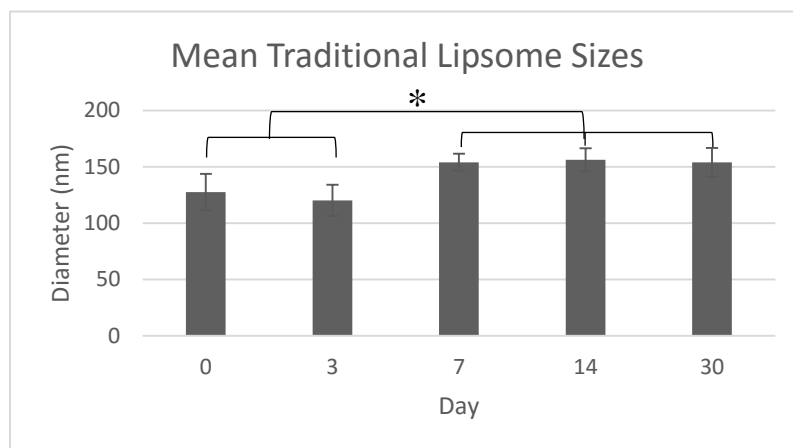
FIGURE 22 –Mean diameter of Traditional Liposomes at various days post-fabrication. *
Denotes statistically different.

The percent changes in mean diameter size from day 0 in each particle type can

be seen in TABLE II. The ethosomes exceed their allowable percent change from day 0

of 34.5% in between days 3 and 7. The ultradeformable and traditional liposomes do not

exceed their predetermined percent change from day 0 of 22.5% and 32.8%, respectively.

TABLE II

PERCENT CHANGE IN PARTICLE MEAN DIAMETER FROM DAY 0

	Percent change in Mean Diameter (%)		
Days	Ethosomes	Ultradeformable Liposomes	Traditional Liposomes
0-3	32.4	2.63	5.65
0-7	74.5	6.80	20.9
0-14	75.7	6.21	22.5
0-30		7.84	20.7
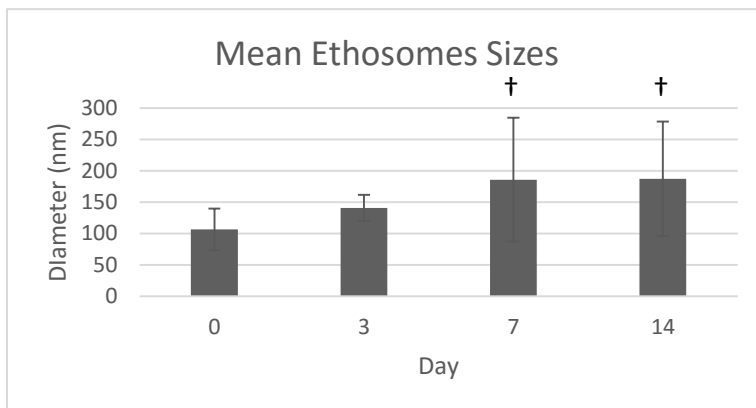
FIGURE 23 –Mean diameter of ethosomes at various days post-fabrication. † denotes percent change from day 0 exceeds predetermined limit.

FIGURE 24 –Mean diameter of ultradeformable liposomes at various days post-fabrication.

In conclusion, the ethosomes initially have the least amount of lipid hydroperoxides compared to the ultradeformable and traditional liposomes. However, change in particle diameter from day 0 exceeds the predetermined limit during the day 3

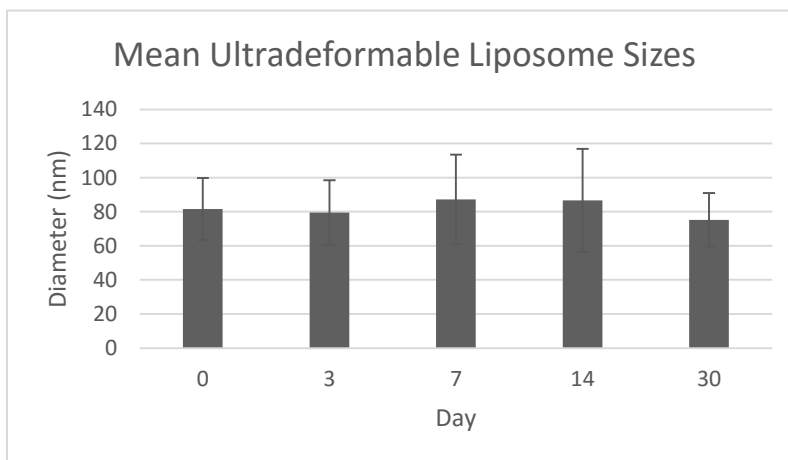and 7 time points. The ultradeformable liposomes have the highest initial amount of lipid hydroperoxides; however, the mean diameters do not significantly change from day 0 to day 30. The traditional liposomes have a statistically significant change in diameter from day 3 to day 7. Therefore, the ethosomes and traditional liposomes are stable until day 3 while the ultradeformable liposomes are stable until day 30.

C. Liposome Characterization Using SEM

An SEM image was used to ensure appropriate particle formation and morphology. FIGURE 24A shows ethosome particle formation, EHT=2.00kV. Ethosomes appear semi-spherical and vary in size. Figure 24B shows the ultradeformable liposomes at an EHT=3.00kV. The ultradeformable liposomes exhibit a smooth and spherical morphology with varying vesicle sizes. The traditional liposomes are shown in Figure 24C at an EHT=2.00kV. They appear to have a semi-spherical formation with varying sizes. The sizes appear to be similar to those established with the DLS.
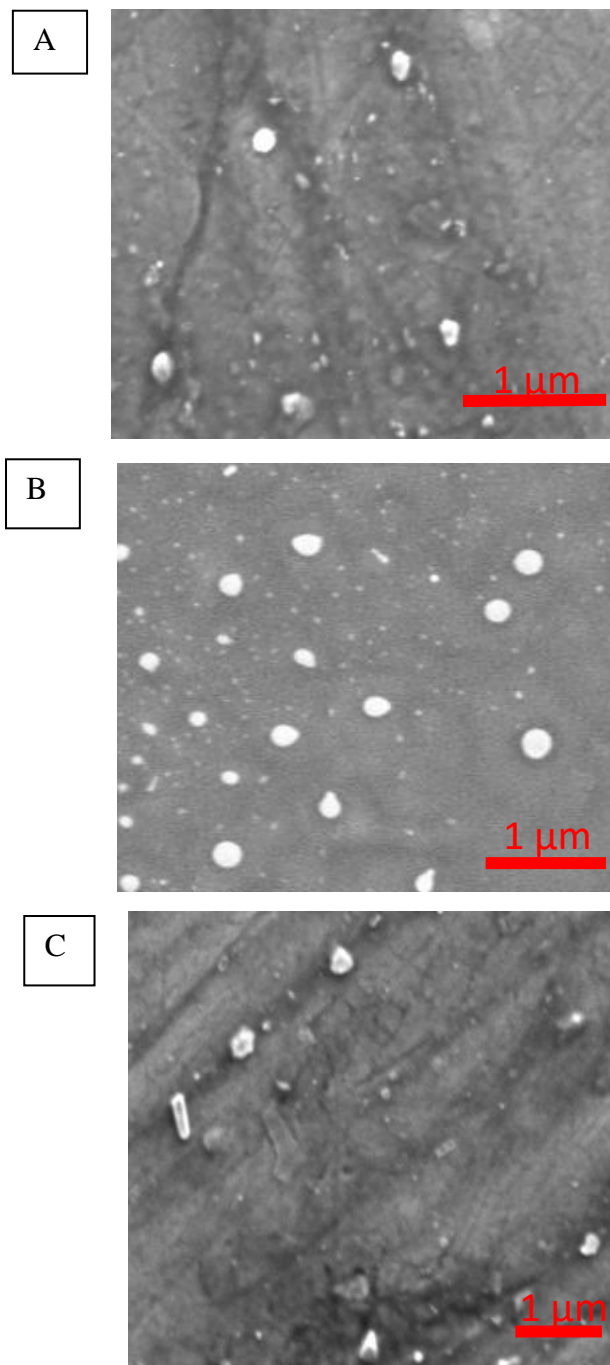
FIGURE 25 – STEM images of (A) ethosomes, (B) ultradeformable liposomes, and (C) traditional liposomes.

D. Entrapment Efficiency

The ultracentrifugation method was used to determine curcumin entrapment efficiency of each particle type. The three absorbance readings from one sample were averaged together. These averages were used to run a one-way ANOVA post hoc Tukey (α=0.05), which determined that vesicle type affects entrapment efficiency of curcumin (p=0.008). Ethosomes had the highest entrapment efficiency of curcumin, 92.4% $\pm$ 4.69%, and was statistically different from the ultradeformable liposomes, 82.1% $\pm$ 5.27% (p=0.001). The traditional liposomes had an entrapment efficiency of 88.1% $\pm$ 3.17%. Traditional Liposomes were statistically similar to the ethosomes (p=0.189) and the ultradeformable liposomes (p=0.061). These entrapment efficiencies yield a true curcumin concentration in the ethosomes of 0.44 mg/ml, in the ultradeformable liposomes of 0.39 mg/ml, and in the traditional liposomes of 0.42 mg/ml.

The entrapment efficiency of N-MPG was calculated theoretically, by taking the percentage of inner vesicle volume over total volume of the sample. The ethosomes had the highest entrapment efficiency of N-MPG of 3.08%. The ultradeformable liposomes had the lowest N-MPG entrapment efficiency of 1.92%. The traditional liposomes had an entrapment efficiency of 2.94%. The ethosomes having the highest entrapment efficiency of curcumin and N-MPG was expected due to their larger hydrodynamic radius. These entrapment efficiencies yield a theoretical N-MPG concentration in the ethosomes of 0.031 mg/ml, in the ultradeformable liposomes of 0.019 mg/ml, and in the traditional liposomes of 0.029 mg/ml.

TABLE III

ENTRAPMENT EFFICIENCY OF CURCUMIN AND N-MPG OF VESICLES

Particle Type	Actual Entrapment Efficiency of curcumin mean ± standard deviation (%)	Theoretical Entrapment Efficiency of N-MPG (%)
Ethosomes	92.4 ± 4.69	3.08
Ultradeformable Liposomes	82.1 ± 5.27*	1.92
Traditional Liposomes	88.1 ± 3.17	2.94

*denotes statistically different.

E. Skin Permeation

In order to quantify skin permeation of the vesicles, a modified Franz Diffusion chamber was created using a 12 well plate and Transwell cell culture inserts to simulate an apical and basal layer of skin. Pig skin was fixed to the cell culture insert and treatments were placed on top of the skin. Absorbance measurements were taken from the media below the insert inside the cell well using a NanoDrop spectrophotometer (Thermo) at various time points. Most of the treatments were too similar to the control PBS readings to detect differences, while the ultradeformable liposomes had extreme and questionable variability. This could be due to machine insensitivity. Also, the surgical glue used to secure the skin samples to the cell culture inserts could have clogged the membrane pores, preventing permeation into the bottom chamber. Curcumin could have also degraded, hindering absorption measurements.
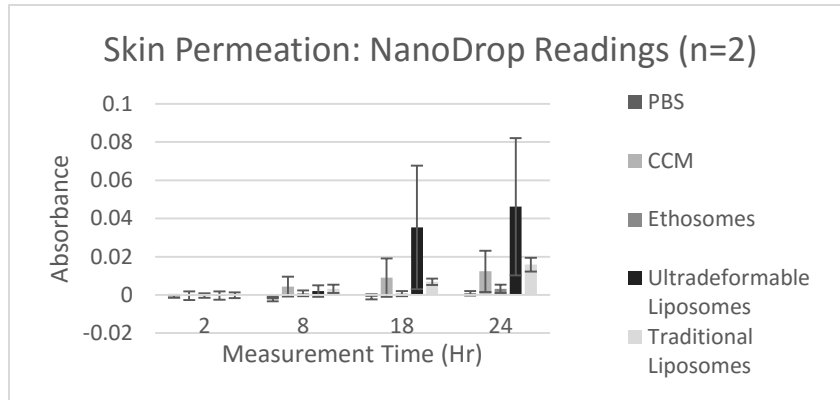
FIGURE 26 –Skin Permeation measurements taken with a NanoDrop.

Therefore, fluorescence was measured using a fluorometer (Turner Biosystems). FIGURE 27 shows these results. Once again, this form of measurement was determined unreliable because of the little difference from the PBS control treatment. Once again, this could be due to machine insensitivity, clogging of pores, or curcumin degradation.

FIGURE 27 –Skin Permeation measurements taken with a Fluorometer.

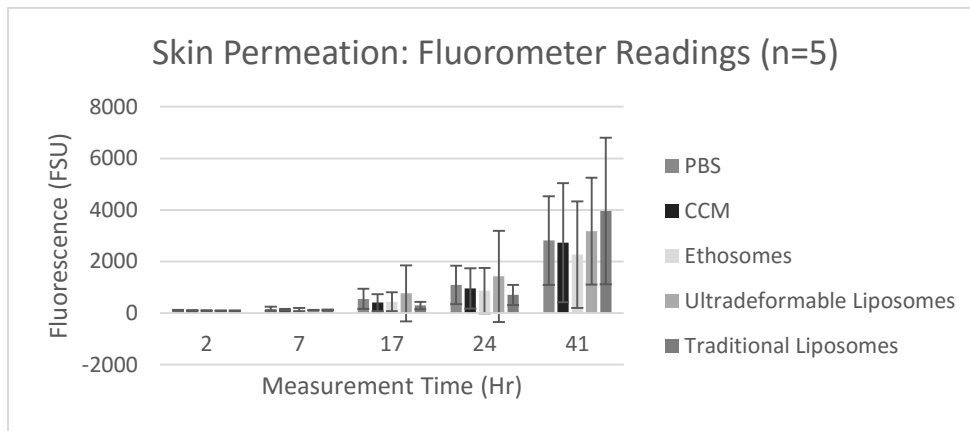Quantifying the amount of vesicles permeating through the skin was proving unsuccessful. Therefore, the amount of vesicles depositing in the skin was quantified. An ultrasonic bath (Fisher Scientific) was used to release the vesicles from the skin. Fluorescence readings were then taken. This was performed applying treatments for 2 and 24 hours. A one-way ANOVA post hoc Tukey ($\alpha=0.05$) showed that particle type significantly affects skin deposition at hours 2 and 24 ($p=0.000$ and $p=0.000$, respectively). At hour 2, all particle types had statistically higher fluorescence then the control PBS treatment ($p<0.000$) as expected. The particle treatment that exhibited the highest skin deposition was the ethosomes ($p=0.000$), followed by the ultradeformable
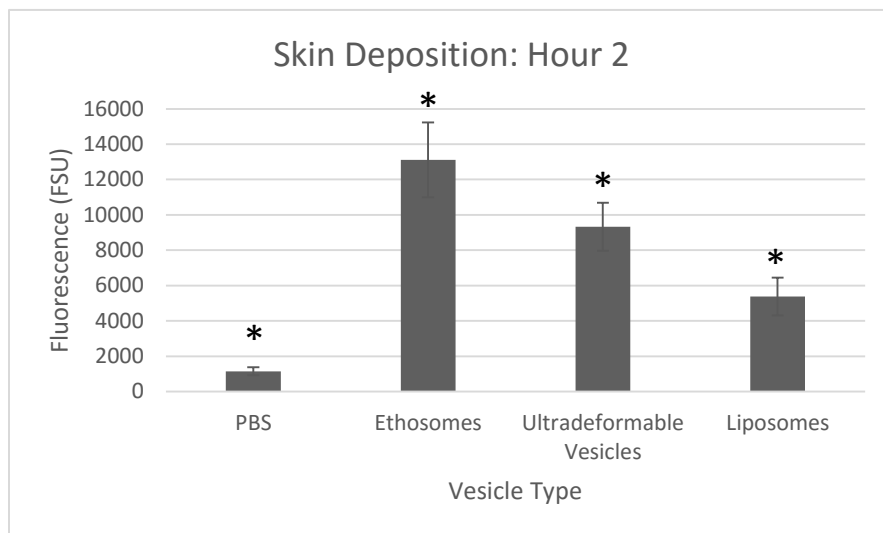

FIGURE 28 –Skin Deposition of vesicles at hour 2. *denotes statistically different.

liposomes. The particle type that had the lowest fluorescence was the traditional liposomes.

At hour 24, the control treatment, PBS, expectedly exhibited the least amount of fluorescence and was statistically different from all other treatments ($p<0.010$). The

particle treatment that had the highest fluorescence was the traditional liposomes, which was also statistically similar to the ultradeformable liposomes (p=0.972). Out of the particle types, the ethosomes had the lowest skin deposition at hour 24.
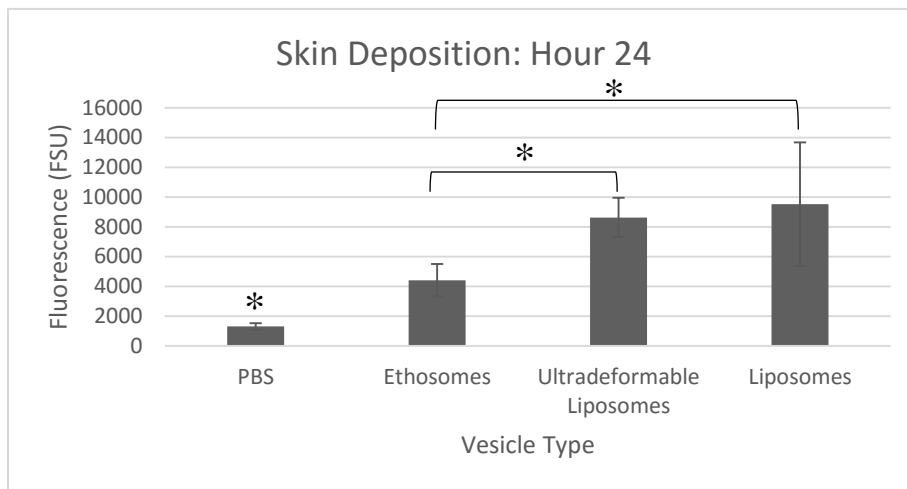
FIGURE 29 –Skin Deposition of vesicles at hour 24. *denotes statistically different.

From the skin deposition results, one can conclude that the ethosomes penetrate the skin faster, while the traditional liposomes and ultradeformable liposomes permeate more slowly. Over time, the permeation of the ultradeformable liposomes and traditional liposomes increases, exceeding the amount of ethosomes permeating.

In order to visualize the particles permeated into the skin, image analysis was performed. An H&E stain was performed to visualize the skin layers and to determine the approximate depth of each layer. Also, any differences in skin structure after the treatments were examined.
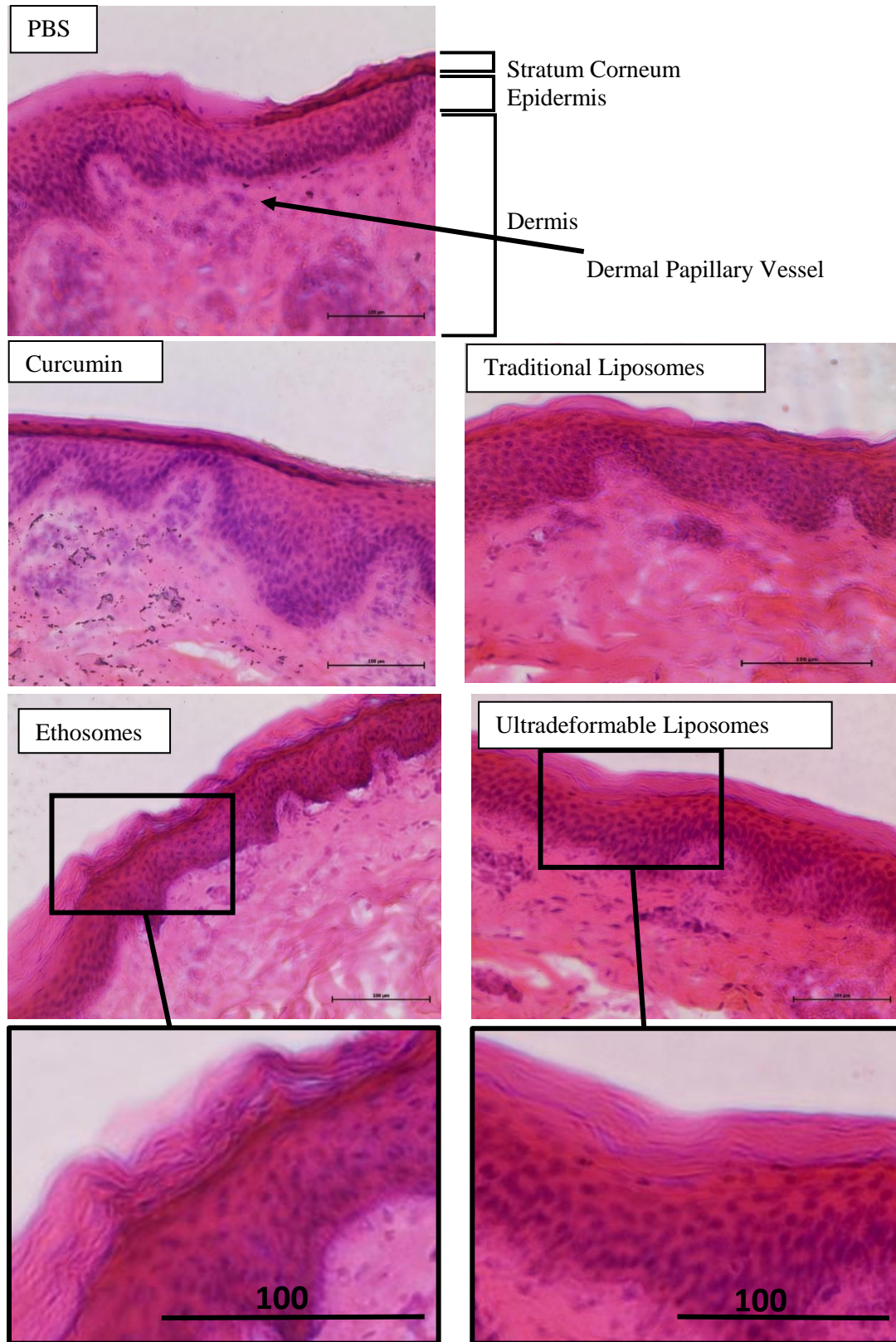
FIGURE 30 –H&E stained sections of treated pig skin, with magnified stratum corneum
of ethosomes and ultraformable liposomes

The average length and standard deviation of the stratum corneum is 25.72 μm ± 9.02 μm. The average length and standard deviation of the epidermis is 61.25 μm ± 21.42 μm. The only visual differences among the treated skin versus the PBS control skin can be seen in the stratum corneum. In the ethosome and ultradeformable liposome treatments, the stratum corneum appears more striated and porous. The depth of the skin layers were then used to analyze the fluorescent images.
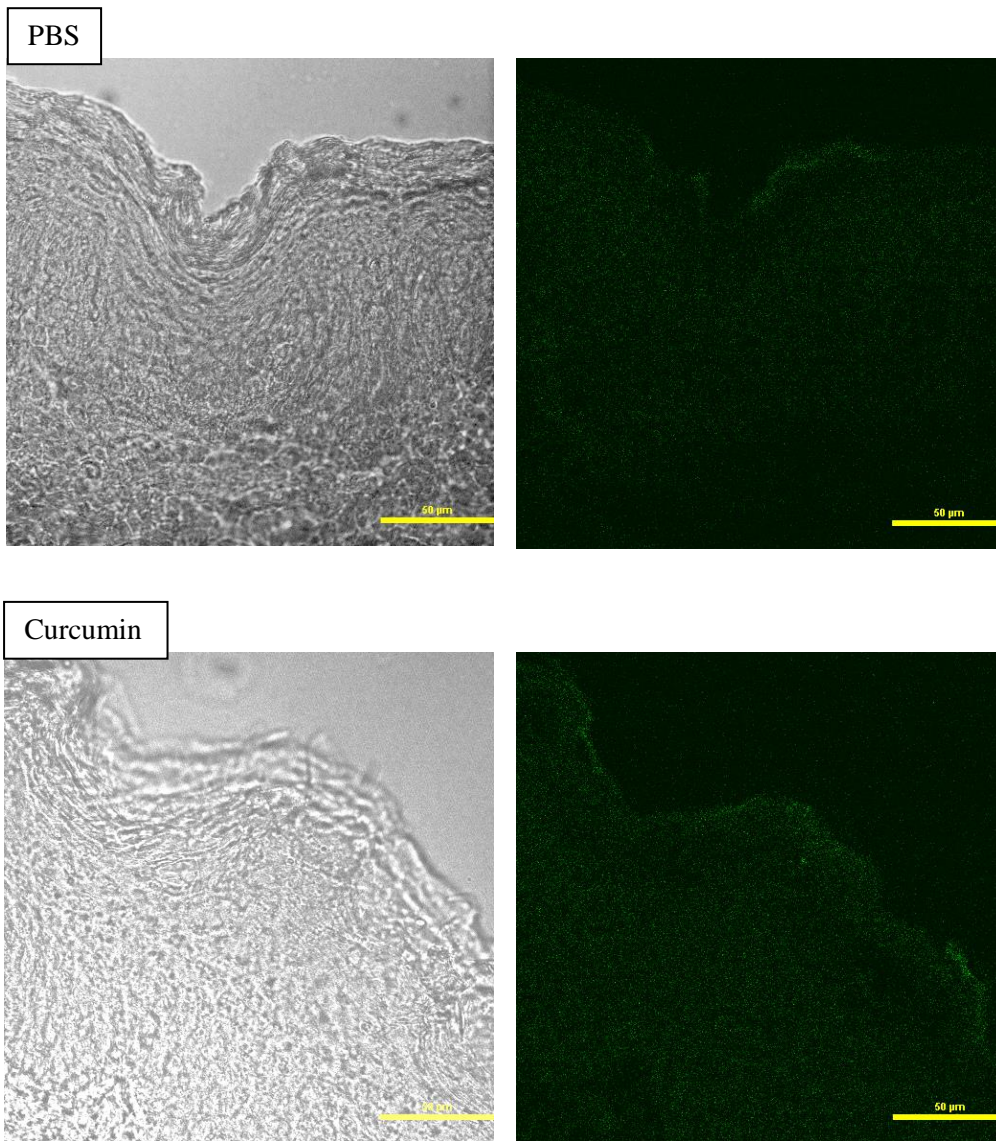
Ethosomes
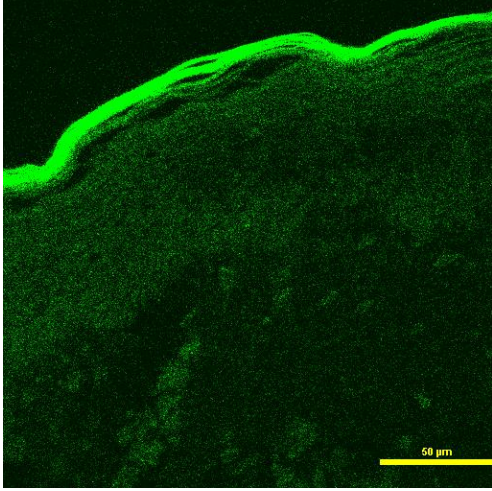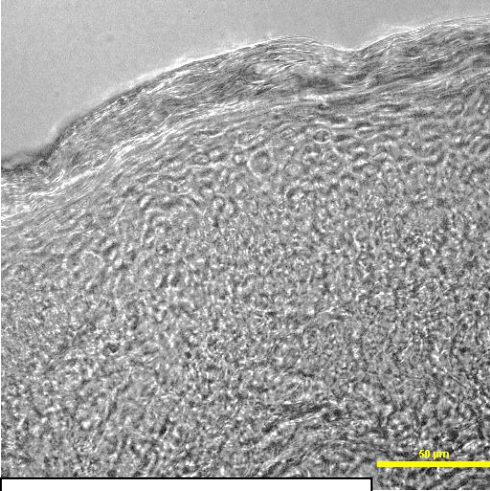
Ultradeformable Liposomes
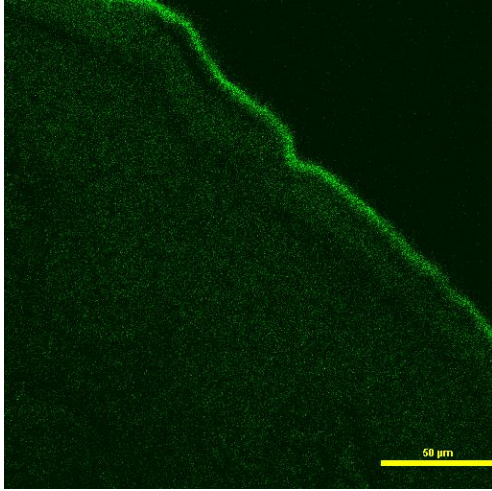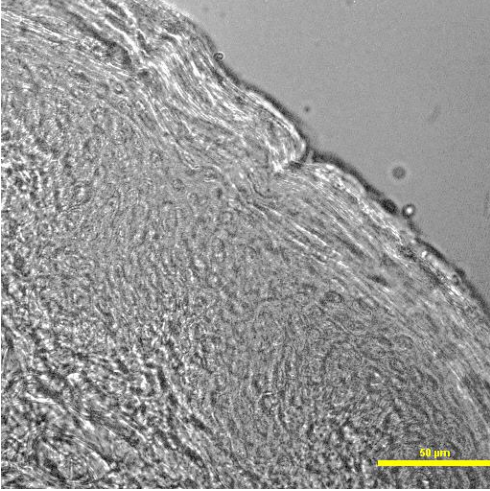
Traditional Liposomes
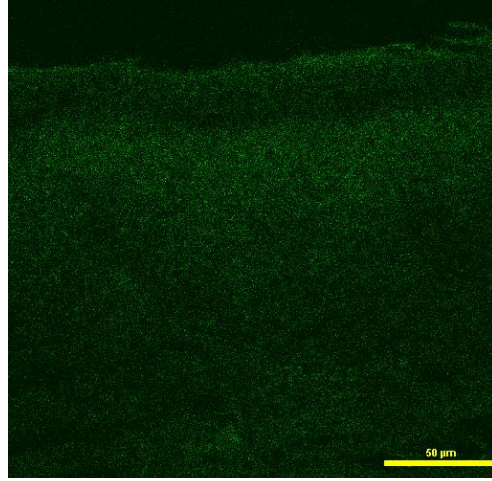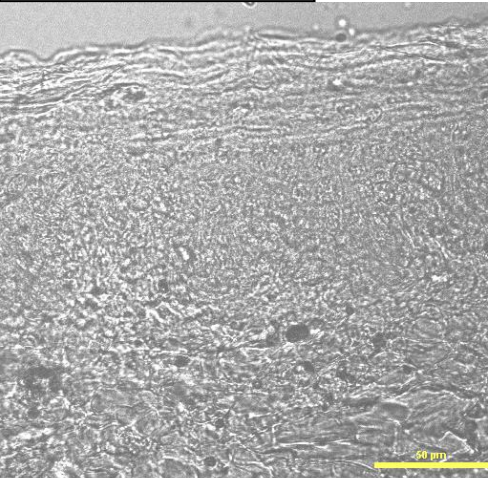
FIGURE 31 –Bright field and GFP images of treated skin.

The fluorescent images were taken using a confocal microscope and analyzed using NIS Elements software. Sum intensity measurements were taken for each skin layer for each treatment. A one-way ANOVA ($\alpha=0.05$) found that particle type significantly affected image sum intensity for the stratum corneum (p=0.001), the epidermis (p=0.000), and the dermis (p=0.000). The curcumin control group was the group with the minimal sum intensity for each skin layer. Equal variance could not be assumed for comparing particle type in the stratum corneum layer (approximately 0-25 μm depth); therefore, a Games-Howell post hoc was used. This analysis showed that the ethosome treated skin had the highest sum intensity and were statistically different from the control curcumin group (p=0.002). The ultradeformable liposomes were the next highest treatment but were not statistically different from the curcumin control group (p=0.203) or the traditional liposomes (0.372). The traditional liposomes were next and weren't statistically different from the control group (p=0.726) or ultradeformable liposomes.

Equal variance could be assumed for the epidermis and dermis layer; therefore, a post hoc Tukey test was used to compare the particle types. In the epidermis layer (approximately 25-86 μm depth), the traditional liposomes maximized the sum intensity and were statistically different from the curcumin control (p=0.000). The next maximizing treatment was the ethosomes which were statistically similar to the traditional liposomes (p=0.149) and the curcumin control (p=0.072). The ultradeformable liposomes were the least maximizing of the particle types and were statistically similar to the control curcumin group (p=1.000). For the dermis layer (approximately 86 μm and greater in depth), a post hoc Tukey showed that the sum intensity for the traditional liposomes maximized the sum intensity and was statistically different from the curcumin

control group (p=0.000). The ultradeformable liposomes were not statistically different from the control group (p=0.350), nor were the ethosomes (p=0.057).
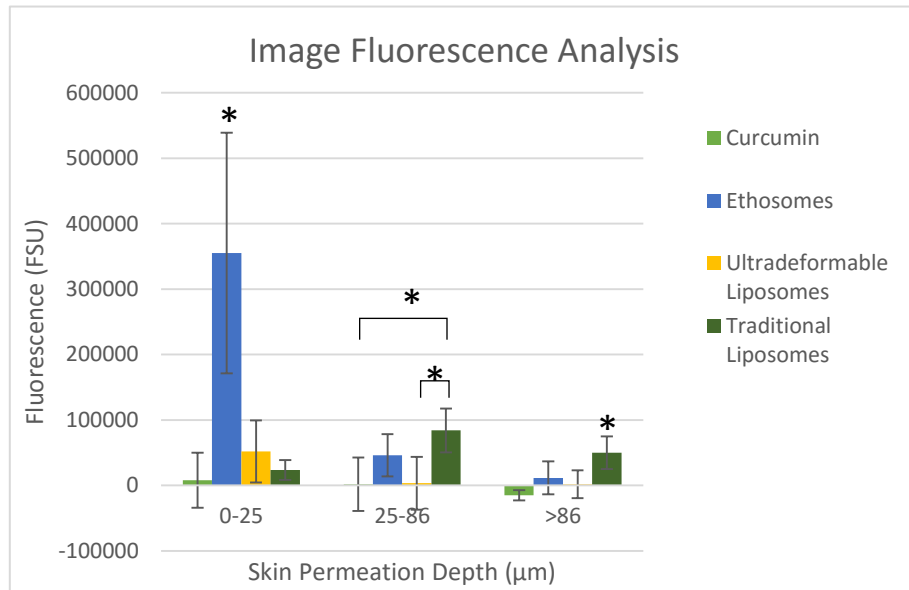
FIGURE 32 –Image fluorescence analysis. Skin permeation depth was obtained from H&E depth measurements. * denotes statistically different.

IV. CONCLUSIONS, DISCUSSION, & FUTURE WORK

In conclusion, three lipid vesicle formulations, traditional liposomes, ultradeformable liposomes, and ethosomes, were designed for combined transdermal delivery of two antioxidants, curcumin and N-MPG. All vesicles were less than 200 nm in diameter and were characterized for stability, morphology, entrapment efficiency, and transdermal delivery.

The ultradeformable and traditional liposomes were fabricated using the mechanical-dispersion method. The ethosomes were fabricated using the cold method and running the particles through a 0.2 μm sterile filter. These fabrication techniques yielded vesicle sizes under the predetermined diameter limit of 200 nm.

The stability of the unloaded vesicles was determined using a PeroxiDetect Kit to analyze the amount of lipid hydroperoxides. The particle type that inherently had the minimal nano-moles of lipid hydroperoxides was the ethosomes, followed by the traditional liposomes. However, from days 0 to 7, all of the lipid vesicles are under the predetermined acceptable limit of 10 nmoles of lipid hydroperoxides. By day 113, all of the lipid vesicles exceeded this limit. A potential issue with the results obtained from the kit is that the phosphate in the lipid vesicle buffers could have interacted with the solutions in the kit to cause higher absorbance readings. Therefore, the results are representative of trends in lipid hydroperoxide formation. Also, the amount of lipid hydroperoxides is expected to be much less with the presence of curcumin and N-MPG, and hence more stable, because the antioxidants can quench their formation.

The stability of the drug-loaded vesicles was also determined by measuring the size of the particle types at various time points. The ultradeformable liposomes did not statistically change in size or exceed the predetermined allowable amount of percent change in size. At day 7, the traditional liposomes were statistically different in size from day 0; however, they never exceeded their allowable percent change in size. The ethosomes were not statistically different in size at measured time points; however, they did exceed their allowable percent change in between days 3 and 7.

The morphology of each particle type was examined using SEM imaging. The ultradeformable liposomes had the smoothest and most spherically shaped vesicles. The ethosomes and the traditional liposomes were semi-spherically shaped, but were not as smooth. The particle type that had the highest actual entrapment efficiency of curcumin was the ethosomes; however, they were statistically similar to the traditional liposomes. The ultradeformable liposomes had the lowest entrapment efficiency of curcumin and N-MPG. The ethosomes, once again had the highest theoretical entrapment efficiency of N-MPG. However, these theoretical entrapment efficiencies of N-MPG are still rather low.

Based on these results, the particles with the best stability and morphology are the ultradeformable liposomes. The ethosomes had the best entrapment efficiency and were statistically similar to the traditional liposomes. For the skin deposition studies, all particle types had statistically higher fluorescence ($\alpha=0.05$) than the PBS control. At hour 2, the ethosomes had the highest fluorescence and were statistically different from all other treatment types. This indicates that the ethosomes have the quickest penetration into the skin. At hour 24, the traditional liposomes had the highest fluorescence and were only statistically similar to the ultradeformable liposomes. This indicates that over time, the

traditional liposomes and ultradeformable liposomes increase in permeation. The decrease in ethosome permeation could be due to particle breakdown because of their relative instability. The pig skin is also potentially degrading, introducing pores, bacteria, and other extraneous factors that could affect the results.

The image analysis showed that the ethosomes had the highest sum intensity in the stratum corneum and were statistically different from the free curcumin control. In the epidermis, the traditional liposomes had the highest sum intensity, were statistically different from the free curcumin control, and also statistically similar to the ethosomes. The traditional liposomes had the highest sum intensity in the dermis and were the only treatment statistically different from the free curcumin control. The ethosomes have the potential to be statistically different from the free curcumin control (p=0.057). Since this image analysis was only performed with an n=1, increasing the number of replicates will provide a better understanding of the potential of each treatment. However, these results strongly indicate that the ethosomes and traditional liposomes permeate into and through the stratum corneum.

For future work, the stability of the ethosomes and liposomes may need to be increased by adding additional lipid soluble antioxidants. While curcumin is a lipid soluble ROS scavenger, the location of the curcumin in the membrane bilayer is similar to cholesterol. In this model, the phenolic hydroxyl groups of curcumin are close to the water penetration space between adjacent phospholipids. The addition of alpha-tocopherol (Vitamin E), a known membrane antioxidant, could decrease ROS production from the unsaturated fatty acids. Another approach is to use a base composition of phospholipids that contains less unsaturated phospholipids. During fabrication, using a

homogenizer as opposed to a probe sonicator to decrease particle size could increase stability as well. Probe sonication introduces ultrasound pulses into the solution, creating excessive particle motion and high heat, leading to the formation of the degrading lipid hydroperoxides. A homogenizer forces the particles through small pores, hence limiting their size without the high temperatures.

Another future PeroxiDetect Assay performed on the particles with the lipids extracted out of their buffer solutions may need to be completed to yield a more true representation of vesicle stability. Also, more image analysis needs to be performed to increase the sample size. The current sample size is just an n=1; therefore, the current result is only a trend and qualitative assessment.

Ultimately, the particle treatments are going to be incorporated into a transdermal patch, and future skin permeation studies will be performed. For applications requiring short-term drug delivery of curcumin and N-MPG, such has a person needing immediate relief from radiation poisoning, the ethosomes seem to be the best particle type. The ethosomes had the quickest skin deposition and with further studies, may prove to reach the deeper skin layers. Unless the stability of these particles are not improved upon, their usefulness for more long-term applications, such as protection from extended radiation exposure, appears to be limited. The particles that seem to be best for these types of applications are the traditional liposomes. They are the particles that had the highest skin deposition at hour 24 and the highest sum Intensity in the dermis skin layer.

LIST OF REFERENCES

[1] Uttara, Bayani et al. "Oxidative Stress and Neurodegenerative Diseases: A Review of Upstream and Downstream Antioxidant Therapeutic Options."*Current Neuropharmacology* 7.1 (2009): 65–74. *PMC*. Web. 23 Dec. 2015.

[2] Bhattacharyya, A., R. Chattopadhyay, S. Mitra, and S. E. Crowe. "Oxidative Stress: An Essential Factor in the Pathogenesis of Gastrointestinal Mucosal Diseases." *Physiological Reviews* 94.2 (2014): 329-54. Print.

[3] Gupta, Subash C., Sridevi Patchva, and Bharat B. Aggarwal. "Therapeutic Roles of Curcumin: Lessons Learned from Clinical Trials." *The AAPS Journal AAPS J* 15.1 (2012): 195-218. Print.

[4] Barzegar, Abolfazl, and Ali A. Moosavi-Movahedi. "Intracellular ROS Protection Efficiency and Free Radical-Scavenging Activity of Curcumin." Ed. Joao B. Calixto. *PLoS ONE* 6.10 (2011): e26012. *PMC*. Web. 23 Dec. 2015.

[5] Priyadarsini, Kavirayani. "The Chemistry of Curcumin: From Extraction to Therapeutic Agent." *Molecules* 19.12 (2014): 20091-0112. Print.

[6] Dutta AK, Ikiki E. "Novel Drug Delivery Systems to Improve Bioavailability of Curcumin." *J Bioequiv Availab* 6 (2013): 001-009. doi:10.4172/

[7] Berginc K, Trontelj J, Basnet NS, Kristl A. "Physiological barriers to the oral delivery of curcumin." *Pharmazie* 67 (2012): 518-524.

[8] Penugonda, Suman, Wei Wu, Suneetha Mare, and Nuran Ercal. "Liquid Chromatography Analysis of N-(2-mercaptopropionyl)-glycine in Biological Samples by ThioGlo™ 3 Derivatization." *Journal of Chromatography B* (2004): 251-56. Print.

[9] Fantinelli, Juliana C., Luisa F. González Arbeláez, Ignacio A. Pérez Núñez, and Susana M. Mosca. "Protective Effects of N-(2-mercaptopropionyl)-glycine against Ischemia–reperfusion Injury in Hypertrophied Hearts." *Experimental and Molecular Pathology* 94.1 (2012): 277-84. Print.

[10] Hercelin, B., et al., "The pharmacokinetics of tiopronin and its principal metabolite (2mercaptopropionic acid) after oral administration to healthy volunteers." *Eur J Clin Pharmacol,* (1992). 43(1): p. 93-5.

[11] "N-(2-Mercaptopropionyl)glycine." *N-(2-Mercaptopropionyl)glycine*. Web. 29 Dec. 2015.

[12] Wu X, Xu J, Huang X, Wen C. "Self-microemulsifying drug delivery system improves curcumin dissolution and bioavailability." *Drug Dev Ind Pharm* 37 (2011): 15-23.

[13] Bisht S, Mizuma M, Feldmann G, Ottenhof NA, Hong SM, et al. "Systemic administration of polymeric nanoparticle-encapsulated curcumin (NanoCurc) blocks tumor growth and metastases in preclinical models of pancreatic cancer". *Mol Cancer Ther* 9 (2010): 2255-2264.

[14] Prausnitz, M. R. and R. Langer. "Transdermal drug delivery." *Nat Biotechnol* 26(11)(2008): 1261-1268.

[15] Prasanthi, D., & Lakshmi, P. "Vesicles-Mechanism of Transdermal Permeation: A Review." *Asian Journal of Pharmaceutical and Clinical Research*, 5(1). (2012)

[16] Kunisawa, J., et al., "Fusogenic liposome delivers encapsulated nanoparticles for cytosolic controlled gene release*." J Control Release*, (2005.) **105**(3): p. 344-53.

[17] Verma, D. "Particle Size of Liposomes Influences Dermal Delivery of Substances into Skin." *International Journal of Pharmaceutics* 258.1-2 (2003): 141-51. Web.

[18] Venkatesh, D. Nagasamy, K. Kalyani, K. Tulasi, V. Swetha Priyanka, S. K. Abid Ali, and H. C. Kiran. "Transfersomes: A Novel Technique for Transdermal Drug Delivery." *International Journal of Research in Pharmaceutical and Nano Sciences* 3.4 (2014): 266-76. Print.

[19] Pratima, Nikalje Anna, and Tiwari Shailee. "Ethosomes: A Novel Tool for Transdermal Drug Delivery." *International Journal of Research and Development in Pharmacy and Sciences* 2.1 (2012): 1-20. Print.

[20] Jyothi, Angadi, Sai Sowjanya, Sreekanth Nama, B. Karuna, and Chandu Babu Rao. "Ethosomes: A Novel Drug Carrier for Transdermal Drug Delivery." *International Journal of Innovative Drug Discovery* 3.1 (2013): 39-44. Web.

[21] "Phospholipids." *We Invest in Quality*. N.p., n.d. Web. 18 July 2016.

[22] Patel, R., S. K. Singh, N.R. Sheth, and R. Gendle. "Development and Characterization of Curcumin Loaded Transfersome for Transdermal Delivery." *Journal of Pharmaceutical Science and Research* 1.4 (2009): 71-80. Print.

[23] Gast, K. and C. Fielder, "Dynamic and static light scattering of intrinsically disordered proteins." *Methods Mol Biol* 896 (2012): 137-61

[24] Akiladevi, D., and Sachinandan Basak. "Ethosomes- a Noninvasive Approach for Transdermal Drug Delivery." International Journal of Current Pharmaceutical Research 2.4 (2010): 1-4. Web.

[25] Celia, Christian, Felisa Cilurzo, Elena Trapasso, Donato Cosco, Massimo Fresta, and Donatella Paolino. "Ethosomes® and Transfersomes® Containing Linoleic Acid: Physicochemical and Technological Features of Topical Drug Delivery Carriers for the

Potential Treatment of Melasma Disorders." Biomedical Microdevices Biomed Microdevices 14.1 (2011): 119-30. Web.

[26] X. Xu, M.A. Khan, and D.J. Burgess. Predicting hydrophilic drug encapsulation in unilamellar liposomes. International Journal of Pharmaceutics (2012) 423(2), pp. 410-418. DOI Link: 10.1016/j.ijpharm.2011.12.019

[27] Son, Joo-Hiuk. "Terahertz Dynamic Imaging of Skin Drug Absorption." *Terahertz Biomedical Science and Technology* (2014): 267-78. Web.

[28] "APPLICATIONS FOR FALCON® CELL CULTURE INSERTS GUIDELINES ..." N.p., n.d. Web. 6 July 2016.

[29] Zhao, Ying-Zheng, Cui-Tao Lu, Yi Zhang, Jian Xiao, Ya-Ping Zhao, Ji-Lai Tian, Yan-Yan Xu, Zhi-Guo Feng, and Chong-Yong Xu. "Selection of High Efficient Transdermal Lipid Vesicle for Curcumin Skin Delivery." *International Journal of Pharmaceutics* 454.1 (2013): 302-09. Web.

[30] "Hematoxylin Stains." *Sigma-aldrich*. N.p., n.d. Web.

Emily Martin

Bardstown, KY 40004 • 502-275-9351 • ekmart01@louisville.edu

EDUCATION

M. Eng. Bioengineering	Aug 2016

J. B. Speed School of Engineering, University of Louisville, Louisville, KY

B. S. Bioengineering	May 2015

J. B. Speed School of Engineering, University of Louisville, Louisville, KY
Graduated with Highest Honors

EMPLOYMENT

<u>University of Louisville</u>

Student Researcher, Department of Bioengineering, Louisville, KY — May 2013- Aug 2016

- Worked on NASA-funded project involving development of drug delivery of antioxidants to mitigate radiation
- Cultured Human Dermal Fibroblasts and Human Promyelocytic Leukemia cells — Aug 2012- April 2013

Student Worker, Vogt Computer Lab, Louisville, KY

- Diagnosed and aided students with computer problems
- Maintained customer service logs and monitored activities in the computer lab

<u>Kentucky Spinal Cord Injury Research Center</u> — Aug 2013- May 2015
Bioengineering Co-op, Louisville, KY

- Designed continuous swimming pool for rats using fluid dynamic principles
- Collaborated with Magnetic Resonance Imaging lab to improve rat spinal cord imaging
- Performed histological staining and analysis to quantify rat spinal cord damage
- Utilized ultrasound technology to determine cardiac output in spinal cord injured rats
- Extensive experience handling and caring for rats

HONORS & AWARDS

Frank & Martha Diebold Humanitarian Award, University of
Louisville

May 2015

**1st Place, Neuroscience Day, Undergraduate poster
competition,** University of Louisville

May 2015

**1st Place, Engineering Expo, Undergraduate poster
competition,** University of Louisville

May 2015

Dean's List, University of Louisville

Various Semesters

ACTIVITIES

BioMedical Engineering Society, University of Louisville   Jan 2013- May 2015

Kickball Team, League of Extraordinary Co-eds, Louisville, KY   May 2014- Present

Intramural Volleyball Team, University of Louisville   Aug 2012- Dec 2013

PUBLICATIONS

**Disruption of locomotion in response to hindlimb muscle
stretch at acute and chronic time points after a spinal cord
injury in rats.**
Keller AV, Wainwright GN, Shum-Siu A, Prince D, Hoeper A,
Martin E, Magnuson DS.

May 2016

In progress

**Challenging Cardiac Function Post-Spinal Cord Injury with
Dobutamine.**
DeVeau KM, Martin EK, King NT, Shum-Siu A, Keller BB, West
C, Magnuson DS.